REVIEW

Review of metal-containing resists in electron beam lithography: perspectives for extreme ultraviolet patterning

Mohammad S. M. Saifullah,[a,*] **Nikhil Tiwale**,[b,*] **and Ramakrishnan Ganesan**[c]

[a]Paul Scherrer Institute, Laboratory for Micro- and Nanotechnology, Villigen, Switzerland
[b]Brookhaven National Laboratory, Center for Functional Nanomaterials, Upton, New York, United States
[c]Birla Institute of Technology and Science Pilani, Department of Chemistry, Hyderabad, Telangana, India

Abstract

Background: Metal-containing resists entered the mainstream semiconductor industry process flow to mitigate the low absorbance of extreme ultraviolet (EUV) radiation by thin films of organic resists that lead to poor sensitivity and their inability to handle rigors of development and etching conditions.

Aim: The long and rich history of using metal-containing resists in electron beam lithography can offer interesting lessons, pointers, and insights to the relatively newcomer EUV lithography, which is slightly over a decade old.

Approach: Electron beam lithography has been enjoying a considerable amount of freedom in the choice of resist materials for close to 50 years; especially the use of metal-containing resists to attain not only single digit nanometer resolution, higher sensitivity, and etch resistance but also lower line-edge roughness. Here, we make a comprehensive historical review of the progress made in the patterning of metal-containing resists in electron beam lithography and derive insights that can be potentially useful in EUV patterning.

Perspectives: Small molecular weight resists are proven to be crucial for achieving higher resolution with low line-edge roughness. Simplifying process flow by reducing etch-stack-layers is conceivable with metal-containing resists, along with direct-patterning of functional materials for heterogeneous integration. Efficient contact hole patterning at tighter pitches may be incumbent on progress in positive-tone resist research.

© *2022 Society of Photo-Optical Instrumentation Engineers (SPIE)* [DOI: 10.1117/1.JMM.21.4.041402]

Keywords: metal-containing resists; electron beam lithography; EUV lithography; nanofabrication.

Paper 21094SSV received Dec. 2, 2021; accepted for publication Mar. 14, 2022; published online Jun. 2, 2022.

1 Introduction

Photolithography has been the torchbearer of fabricating devices in a micro- and nanometer regime in the semiconductor industry. It uses a resist, a photosensitive polymeric material, for imaging and pattern transfer to a substrate either *via* the process of plasma etching or by lift-off after metal (oxide) deposition. Since 1960s, the technological progress in photolithography, usually "defined" in terms of the Moore's Law, has been uninterrupted, and relentless in pursuing miniaturization of critical device dimensions. The pursuit of ever-shrinking critical dimensions from a few microns in 1960s to ~20 nm in recent times has been made possible by adopting increasingly shorter wavelength imaging radiation (193 nm since early 2000s) coupled with some technological ingenuity in the last decade such as immersion lithography and multiple

*Address all correspondence to Mohammad S. M. Saifullah, msm.saifullah@psi.ch; Nikhil Tiwale, ntiwale@bnl.gov

exposure patterning. In other words, the resolving potential of 193 nm immersion lithography tool has remained almost constant over the years and further shrinking of critical dimensions has been enabled by subsequent processing, which does not come without enormous design complexity and throughput bottleneck. Achievement of higher resolution from a simpler direct photoexposure comes at a large increase in capital cost as it needs shorter wavelength imaging radiation and a suitable resist to take its advantage. These are the two key technologies that are going to power the engine of next-generation semiconductor high volume manufacturing.

In recent years, extreme ultraviolet (EUV) technology (13.5 nm wavelength) has emerged as the strong alternative to ArF immersion lithography for high volume manufacturing.[1,2] Taking advantage of the EUV light source, which suffers from limited power, requires development of resist materials that possess high sensitivity at this wavelength, capable of high resolution, exhibit low line edge roughness (LER), and at the same time preserving the pattern fidelity and uniformity. Chemically amplified resists (CAR), which are primarily organic, have served very well in 248- and 193-nm lithography but are very transparent in EUV wavelength. This represents a major problem as it leads to the reduction of sensitivity of these resists. Exploiting several strategies such as increasing the quantum yield *via* improving acid generation efficiency, perfluorinated photo-acid generators (PAGs), acid amplifiers, photosensitizer along with limiting the acid diffusion by polymer-bound PAGs, and photo-decomposable base quencher, CARs have been able to meet the current 0.33NA EUV lithography requirements.[3–5] However, the dilemma of resist thickness for sufficient absorption versus pattern collapse at high aspect ratio and LER originating from compositional inhomogeneity remains a challenge, and it is only likely to become more stringent with the move toward 0.55NA capabilities. On the other hand, incorporation of certain metals in thin resists leads to high EUV absorbance resulting in improved sensitivity, mitigation of photon-shot-noise effects, and at the same time serve as a durable etch mask. Furthermore, thin resist films also reduce the capillary force-induced resist collapse during development that is common in CAR systems patterned at higher resolution. For these reasons, new resists containing atoms that show increased absorbance at the EUV wavelength have been put forth as a substitute for CARs. In recent years, several reviews have appeared in the literature that discuss the evolutionary progress in resist development in EUV lithography with emphasis on metal-containing resists due to their stated advantages.[6–13]

Unlike at the previously used photolithography wavelength of 193 nm (~6.4 eV, lower than the ionization energy of the resists ~10 eV), where the absorbed radiation can only excite bound states of the chemical bonds, EUV radiation (92 eV) is readily absorbed by the deep valence or shallow–core electrons leading to ionization of the resist and open up a cascade of new reaction pathways.[14] As these semicore excitations are often localized to the resist atoms, it is easy to fathom that inclusion of inorganic/metallic atoms into the resist composition can improve their absorption of EUV radiation; however, that is only half the story. The secondary electrons generated by these atoms, after absorbing the radiation, are in fact the ones driving the necessary solubility change to produce patterned features.[15] It may be less than optimal to simply focus on the former without understanding of the latter.[16] As such, a retrospective look at the studies focused on metal-containing resists used for electron beam lithography is warranted.

Metal-containing resists are relatively new entrants in EUV patterning; however, their use in electron beam lithography has close to a 50-year long history. The availability of intense and small electron probes in the latter half of twentieth century in Vacuum Generators HB5/501HB dedicated scanning transmission electron microscope (VG-STEM) and field emission gun-equipped scanning electron microscope (FEG-SEM) enabled the rise of patterning of nanoscale features directly in a film of ionic materials of low molecular weight to study the ultimate limits of nanofabrication. In late 1990s, a breakthrough in spin-coatable metal oxide resist whose electron beam sensitivity was $>10^6$ times higher than ionic materials—a paradigm shift—that enabled patterning of metal oxides at a single digit nanometer scale on silicon substrates using commercial electron beam writers. Subsequent period demonstrated great freedom in the use of various metals with different moieties leading to direct writing of functional materials. In this paper, we give a comprehensive historical review of the use of metal-containing resists in electron beam lithography and discuss how they directly or indirectly influenced EUV lithography. Furthermore, we believe that the former technique has lessons to offer the latter when it comes to

attaining very high resolution using low molecular weight resists, simplification of lithographic process, direct writing of a host of functional materials, and obtaining low LER.

2 Metal-Containing Resists in Electron Beam Lithography: An Overview

The identification of poly(methyl methacrylate), PMMA, as a high-resolution electron resist in 1968,[17] and its subsequent use to produce the first operational electronic devices in 1970 *via* the lift-off step was a watershed in the history of lithography.[18] Operational devices way beyond the capability of photolithography were shown to be possible. The prefix of "nano" to lithography was attached for the first time when Broers demonstrated 8-nm Au-Pd lines using a contamination resist[19] and showed 25-nm lines with PMMA.[20] These developments spurred the quest for improving the patterning resolution below 10 nm using metal-containing resists of low molecular weight of ∼100 daltons to which we will turn our attention to.

2.1 *Inorganic Resists Based on Metal Halides and Metal Oxides*

2.1.1 *Self-developing metal halide resists*

In 1978, Broers et al. demonstrated holes of 5 nm in diameter in a 250-nm-thick NaCl film using a focused electron probe in an STEM equipped with a LaB_6 filament.[21] The formation of holes was attributed to sublimation of material, and it required an exposure dose of $0.1\ C/m^2$. In 1981, using an intense 0.5 nm probe in a VG HB5 STEM, Isaacson and Muray studied the drilling mechanism in thinner NaCl crystalline films evaporated on carbon support grids.[22] They were able to drill holes of 2 nm diameter and fabricate troughs that were 1.5 nm wide. Although impressive, these were not permanent structures due to the attack of NaCl by atmospheric water vapor. However, this study stimulated research in testing many metal fluorides as high-resolution electron beam resists.

In an 80-nm-thick film of AlF_3, Muray et al. found that an electron dose of $\sim 10\ C/cm^2$ was required to remove aluminum and fluorine from the irradiated areas.[23] Using AlF_3 film as an etch mask against reactive ion etching in a CHF_3 plasma on a 50-nm-thick silicon nitride membrane and subsequent removal of AlF_3 with an aqueous solution of HCl, patterns with dimensions of 8×10 nm were obtained. Since the resist required no further development after the exposure, it was termed as a "self-developing resist." Further studies on AlF_3 resist demonstrated both positive- and negative-tone behavior.[24] Interestingly, it was found that in the irradiated areas, metallic aluminum was formed at doses as low as $\sim 2\ C/cm^2$. Aluminum wires about 20 nm wide were produced by subsequently dissolving the resist in water.

Different metal halides demonstrate different damage mechanisms when irradiated with an intense electron probe [Figs. 1(a) and 1(b)]. Kratschmer and Isaacson investigated a host of metal fluorides such as AlF_3, FeF_2, BaF_2, SrF_2, LaF_3, CrF_2, and CsF for both positive- and negative-tone behavior.[27] Independently, using an STEM, Scherer and Craighead also showed that BaF_2 and SrF_2 films could indeed act as negative-tone resists.[28] Using *in situ* electron energy loss analysis, they observed that both BaF_2 and SrF_2 show a decline in the fluorine K-edge signal during the irradiation, with a simultaneous increase in the oxygen K-edge intensity—the source of oxygen being the vacuum of the microscope chamber. Feature sizes of about 100 nm were achieved on GaAs, with grain size of the resist film acting as a limit factor to achieve higher resolution. Scherer et al. attempted to optimize resolution of the negative fluoride resists by grain size control, which was achieved by alloying SrF_2 film with 8% AlF_3.[29] Other group II metal fluorides such as CaF_2 and MgF_2 were used as positive resists and developed in water or other suitable agents to chemically strip radiolysis-induced products. Mankiewich et al. achieved 30 nm resolution with CaF_2 inorganic resist.[30] When exposed inside an STEM (pressure $\sim 5 \times 10^{-7}$ Torr), radiolysis of CaF_2 led to the formation of CaO as the end product. They suggested that electron beam-induced radiolysis of CaF_2 leads to the formation of Ca metal first, which rapidly oxidizes to CaO by residual oxygen inside the chamber. This chemical conversion required a total dose of $10\ C/cm^2$. Water was used as a developer because CaO is about hundred times more soluble in water than CaF_2. Zanetti et al. continued the work on CaF_2 as an etch

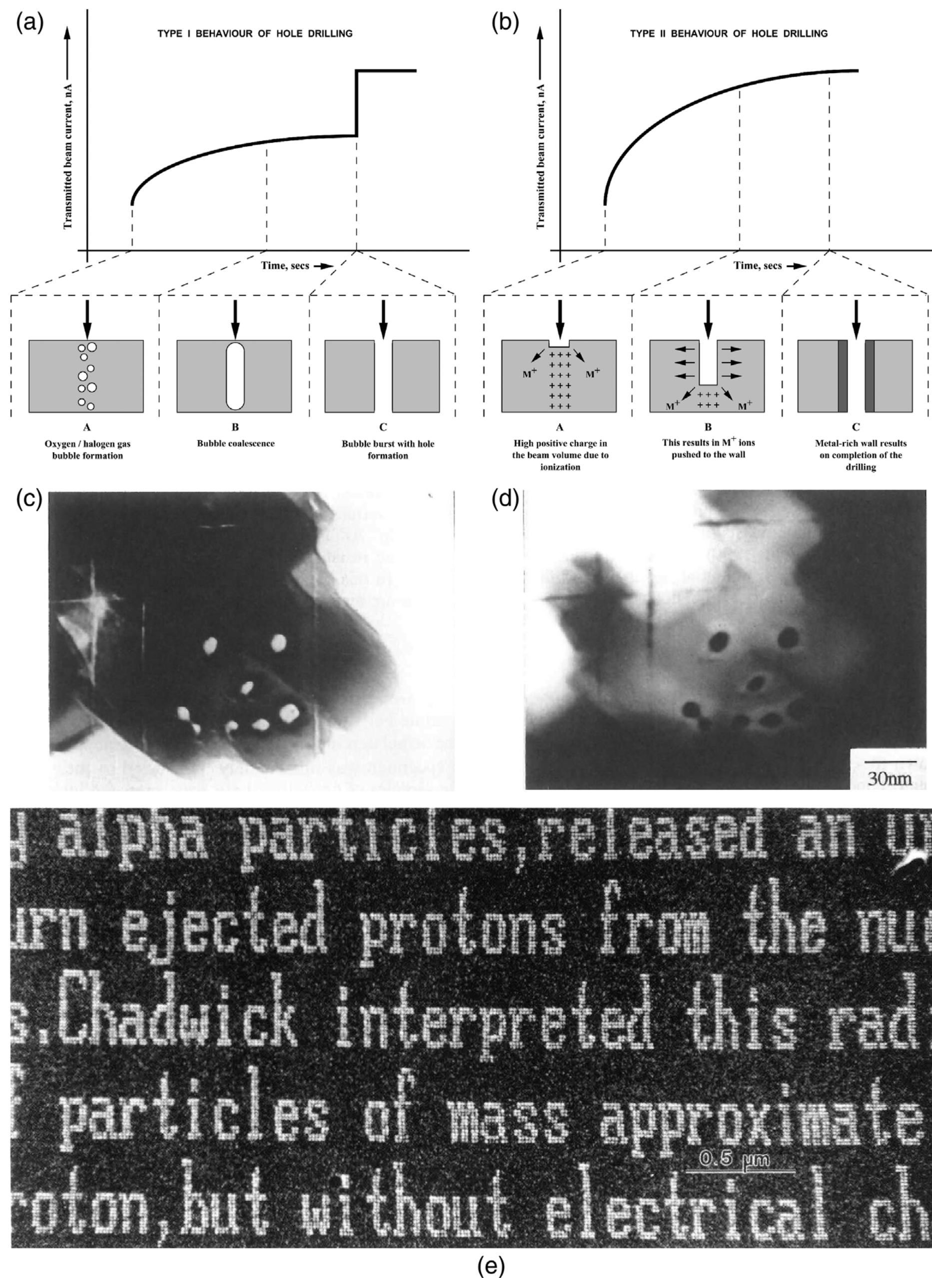

Fig. 1 Drilling curves are transmitted current versus time curves that indicate the mass loss behavior of metal halides and oxides during the exposure to an electron beam. (a) Type I: Here, the gas bubbles form in the irradiated volume, coalesce together, and they "pop" to form a hole after exposure to sufficient electron irradiation. Metal cations are displaced from the irradiated volume to surround the hole. Drilling time shows a nearly linear behavior with accelerating voltage and is relatively temperature and thickness independent. Examples include many amorphous halides and oxides including AlF_3, FeF_3, and Al_2O_3. (b) Type II: Here continuous mass loss is observed during drilling. Material may be lost from both surfaces of the specimen. Drilling time shows highly nonlinear accelerating voltage dependence, but mass loss is accelerated at higher temperatures. Examples are mainly crystalline halides and oxides including CaF_2, TiO_2, FeF_3, NaCl, MgO, and sodium β-alumina. (c) Bright-field and (d) annular dark field images of ∼4 nm lines and ∼8 to 10 nm wide holes machined in crystalline FeF_3 inside a VG 501HB STEM. Notice that the metal pushed to the walls of the holes provides a darker contrast in bright-field and vice versa (from Ref. 25). (e) *Encyclopaedia Britannica* on a pinhead. A portion of Encyclopaedia written in amorphous AlF_3; each hole corresponds to 4 nm in diameter (from Ref. 26). The figure reproduces a part of page 706 of *Encyclopaedia Britannica* referring to Chadwick (*Micropaedia*, Vol. II, Bibai to Coleman. 15th edition, Helen Hemingway Benton: Chicago and London, 1979).

mask.[31] Instead of a simple thermal evaporation, they used molecular beam epitaxy to deposit CaF_2 as a resist on GaAs. Epitaxial CaF_2 films were attained due to a good lattice match between them. Electron energy loss spectroscopy (EELS) studies on crystalline and amorphous FeF_3 by Saifullah et al. showed a decline in the fluorine K-edge signal during electron irradiation, with the F:Fe ratio settling to a value of ∼1.3 [Figs. 1(c) and 1(d)].[25]

The return of FEG-SEM instead of STEM to perform sub-10 nm electron beam lithography marked an important milestone in self-developing metal halide resists. Taking a cue from the earlier work by Langheinrich and Beneking who demonstrated ∼3 to 4 nm resolution in a STEM using AlF_3-doped LiF inorganic resist;[32] in 1995, Fujita et al. using the same resist, demonstrated 5-nm linewidth patterns with 60 nm periodicity on a silicon substrate using a 30-kV electron beam inside an FEG-SEM.[33] Electron stimulated desorption studies suggested the formation of a metal-rich layer by preferential desorption of fluorine. This process suppresses further desorption of fluorine. Self-developing reaction in this resist is achieved by the surface diffusion of the residual metal film.[34]

Despite their very high resolution, metal halides as electron beam resists suffered from couple of disadvantages—their high hygroscopicity and very high dose requirement to either drill a hole or expose the resist. These drawbacks were somewhat alleviated using metal oxides as high-resolution resists, on which we will focus our attention.

2.1.2 *Self-developing metal oxide resists*

Using a highly intense focused electron beam in a VG HB5 STEM, Mochel et al. were able to drill 2-nm holes and cut 2-nm lines through a 200-nm-thick crystalline sample of sodium β-alumina in a few seconds.[35] This was a permanent hole drilling as opposed to what was observed in many metal halides where the holes got "healed" when exposed to the ambient. Furthermore, a stable partially formed hole could be observed if the electron irradiation was stopped before the hole was completely drilled. The hole drilling phenomenon was followed by monitoring the transmitted current versus time. It was observed that the initial constant mass loss was followed by a decrease in the mass loss rate, ending with the formation of a hole [Fig. 1(b)]. The hole drilling process in crystalline sodium β-alumina was further studied by Berger et al. who used EELS and energy filtered imaging, together with transmitted current versus time curves.[36] Using the information obtained from these techniques, they suggested that electron irradiation resulted in the removal of material atom plane by atom plane from both the surfaces during hole drilling. The incident beam also led to ionization, which resulted in desorption of oxygen, with aluminum migrating to the sides of the hole. Devenish et al. used a standard thermionic source in a conventional TEM to drill holes in sodium β-alumina.[37] Salisbury et al. coined the acronym SCRIBE (subnanometer cutting and ruling by an intense beam of electrons) to differentiate the process of hole drilling or "machining" in inorganic materials from conventional electron beam lithography using organic resists.[38]

Among metal oxides, amorphous Al_2O_3 was perhaps the most popular material that was studied using SCRIBE. Studies by Mochel et al.[35] and Berger et al.[36] demonstrated that hole drilling at a nanoscale in an anodized amorphous Al_2O_3 takes place differently from what was observed in crystalline sodium β-alumina. The transmitted current *versus* time showed a quick increase in current followed by a plateau region that increases slowly until the current jumps to a final value [Fig 1(a)]. In other words, amorphous Al_2O_3 undergoes a small but quick mass loss initially followed by a pause during which no mass loss occurs. Finally, an abrupt transition to a hole takes place. Interestingly, it was observed that if the beam was switched off in the plateau region, then the partially drilled hole healed up quickly with no observable sign of the incomplete hole. Using a conventional tungsten thermionic source in a conventional TEM, therefore at a lower current density, Devenish et al. attempted to drill amorphous Al_2O_3.[37] It was observed that at room temperature, the Al_2O_3 film suffered some damage, but no holes could be drilled. However, at liquid nitrogen temperature, holes were easily drilled. A possible explanation for this observation is that at low temperatures, gases such as water vapor and oxygen in the TEM column may be condensed or adsorbed on amorphous Al_2O_3. The electron beam ionizes the adsorbed species, which then participate as reactive ions to boost the hole drilling. Just like what was noticed earlier for anodized amorphous Al_2O_3, some partially drilled holes were also

observed to heal up in amorphous Al_2O_3. It was suggested that the drilling process was a balance between outward electron-beam-induced migration and inward back diffusion of aluminum back, which tends to fill up the hole. Lowering the temperature should decrease the rate of back diffusion of aluminum and hence increase the drilling rate.

Studies by Hollenbach and Buchanan showed that radio frequency sputtered thin films of amorphous Al_2O_3 in a VG HB5 STEM showed significant increase in sensitivity when compared with anodized Al_2O_3 films.[39] The hole formation time in a 90-nm-thick sputtered amorphous Al_2O_3 could be reduced to 50 ms (rather than tens of seconds), and dose requirement for 5 nm wide holes was determined to be $2.5 \times 10^3\ C/cm^2$. The reduction in dose requirement was attributed to the microstructural characteristics and incorporation of a relatively larger atom of argon acting as a structural modifier in the sputtered film. Thus, the faster rate of removal of material from the irradiated area could be due to the more open structure of the amorphous material, leading to increased diffusion rates of atoms. Similar hole drilling results were also obtained for sputter-deposited amorphous films of Y_2O_3, Sc_2O_3, $MgO \cdot Al_2O_3$, and $3Al_2O_3 \cdot 2SiO_2$. Morgan et al. investigated this material further and found that electron irradiation with a high magnification raster (>500 k) causes the holes to heal up.[40] Interestingly, when the holes were drilled closer together than the critical separation, a proximity effect was observed causing the holes to become pear-shaped. On the contrary, crystalline Al_2O_3 did not show these effects.[41]

While studying the SCRIBE process in MgO smoke cubes, Salisbury et al. found that it is possible to "machine" holes and steps on the nanometer scale on the surface of MgO with {100} faces oriented parallel to the electron beam.[38] Further investigations by Turner et al.[42] and Devenish et al.[43] have demonstrated the formation of atomically smooth surface faces when a finely focused beam is rastered over the surface of a MgO crystal. Energy dispersive x-ray spectroscopy during "machining" showed a constant Mg:O ratio suggesting that the material is removed in stoichiometric groups.

Berger et al. observed that hole drilling in TiO_2, TiO, and Ti_2O_3 was similar to that seen in metal β-aluminas—a gradual loss of oxygen and displacement of titanium under the beam.[44] However, the holes did not penetrate through the films and the hole drilling stopped when a critical Ti:O ratio was reached. A comparative study of "machining" of amorphous and crystalline TiO_2 films using a finely focused beam of electrons by Saifullah et al. showed a surprising result—the latter more amenable to hole drilling than the former.[45] Time-resolved EELS studies showed that both amorphous and crystalline TiO_2 films lose oxygen continuously during the exposure to a finely focused electron beam with the final composition settling close to that of TiO.

SiO_2, although not exactly a metal oxide and slightly less ionic than other oxides discussed so far, is also amenable to the SCRIBE process. Using windowless energy dispersive x-ray spectroscopy and EELS studies, Chen et al.[46] and later Saifullah et al.[47] showed that electron beam evaporated self-supporting thin films of SiO_2 can be directly reduced to silicon with an intense 100 kV electron probe inside a VG 501HB STEM. Columns of silicon as small as 2 nm wide were fabricated at an electron dose $>3.0 \times 10^5\ C/cm^2$. During the exposure, both silicon and oxygen are lost, the former more slowly than the latter. Using an intense electron probe in FEG-SEM, Fujita et al. exposed a thermally grown SiO_2 on an Si (111) substrate.[48] This resulted in the formation of SiO, which was selectively thermally desorbed inside an ultrahigh vacuum chamber to produce 10-nm-wide open windows. Pattern transfer produced Si wires of 10 nm width.

Other oxides studied for electron beam-induced hole drilling were ZnO crystals,[38] MoO_3, and $YBa_2Cu_3O_7$.[37] Hole drilling in ZnO crystals gave rise to faceted holes, but the indentation formed equally at both entrance and exit surfaces. In $YBa_2Cu_3O_7$, electron irradiation gave rise to the loss of oxygen, thus transforming it into a semiconductor. Devenish et al. suggested that Josephson junctions could be potentially produced on a nanoscale using the SCRIBE technique.[37] Pauza et al. used electrons to create a narrow damaged section on $YBa_2Cu_3O_7$ film and showed that weak links can be written directly on this material.[49]

With the rare exception of a few studies, almost all the work on metal oxides (and metal halides) as self-developing electron beam resists were carried out using free-standing thin films or nanoscale particles of oxides inside a dedicated STEM. To gain a better understanding of the electron beam exposure behavior of self-developing inorganic resists on a substrate, Saifullah et al. conducted systematic studies using sputtered Al_2O_3 resist on a silicon substrate inside an STEM.[50] By monitoring the changes taking place in the resist as a function of electron dose using

EELS spectra, they noticed that even though both aluminum and oxygen are lost from the irradiated area, a very thin film of consisting of aluminum and oxygen remains. Even a prolonged exposure did not remove this film. Amorphous Al_2O_3 is resistant to reactive ion etching in fluorine-containing plasmas. Presence of small amount of amorphous Al_2O_3 on the substrate can result in the lack of pattern transfer.

2.1.3 *Electron beam damage mechanisms in inorganic resists based on metal halides and metal oxides*

Electron beam damage mechanisms involved during the SCRIBE process of inorganic resists based on metal halides and metal oxides are varied with different mechanisms dominant in different materials (Fig. 2). Here, we summarize them.

- Radiolysis: This process occurs with relatively high efficiency in alkali and alkaline earth halides as well as other inorganic materials [Fig. 2(a)].[51] It can be considered as the main damage mechanism in the SCRIBE process.[23,27,30,35] Models by Pooley,[52] and later by Kabler and Williams[53] suggest that in alkali halides, decay of excitons could transfer their energy to induce molecular dissociation leading to the formation of an F center (i.e., halogen vacancy).
- Knock-on displacement: This happens by direct momentum transfer from an incident electron to the atomic nucleus. When the energy transferred to an atom is greater than the threshold energy for knock-on displacement, this results in the displacement of a lattice atom from its normal site giving rise to an interstitial vacancy Frenkel pair defect [Fig. 2(b)]. The threshold energy leading to Frenkel pair defect depends upon the bond strength, orientation of the crystal with respect to the incident electrons, space available for accommodating an interstitial atom in the lattice, the form of interstitials, and specimen temperature. Due to reduced interatomic bonding of molecules at or near surfaces, they are more susceptible to displacement due to direct momentum transfer. Surfaces can also be rendered unstable when irradiated with an electron beam.
- Knotek–Feibelman mechanism: This model describes how the excitation of core levels followed by an interatomic decay leads to surface desorption of materials.[54,55] In materials such as TiO_2, Knotek and Feibelman observed that if an electron is removed by ionization from Ti then an intermediate Auger process can cause the loss of up to three electrons from an O^{2-} ion to give an O^+ ion. This creates repulsion in the lattice leading to desorption of oxygen [Fig. 2(c)].

Mochel et al. proposed that in crystalline sodium β-alumina, oxygen was desorbed via the Knotek–Feibelman mechanism, and aluminum migrated to the sides of the hole during "machining" with a focused beam of electrons.[35] This model was also reiterated by Humphreys et al. for hole drilling in Al_2O_3, where 2p, the highest occupied level of the Al^{3+} ion, is deep enough to provide energy to remove one or two electrons from O^{2-}.[26]

2.1.4 *Outlook on inorganic resists based on metal halides and metal oxides*

In Sec. 2.1, we noted that electron beam lithography using inorganic resists was carried out using a dedicated STEM and membrane–film substrate. It successfully demonstrated single digit nanometer resolution as small as 2 nm. Utilizing the high resolution offered by AlF_3 resist and taking a cue from the question posed by Richard Feynman "Why cannot we write the entire 24 volumes of the Encyclopaedia Britannica on the head of a pin?" in his paper titled "There's Plenty of Room at the Bottom,"[56] Humphreys et al. demonstrated that the writing of contents of the *Encyclopaedia Britannica* on a pinhead is indeed possible.[26] They also pointed out that if the letters are represented by a code of dots and dashes in patterned AlF_3 resist then the contents of the *Encyclopaedia* would fit on a pinhead with plenty of room to spare [Fig. 1(e)]. Another advantage of inorganic resists is that they are usually self-developing and require little or no chemical development post-exposure. However, they suffered from a steeper requirement of electron dose, especially when they were patterned on a solid substrate.[50] Moreover, the use

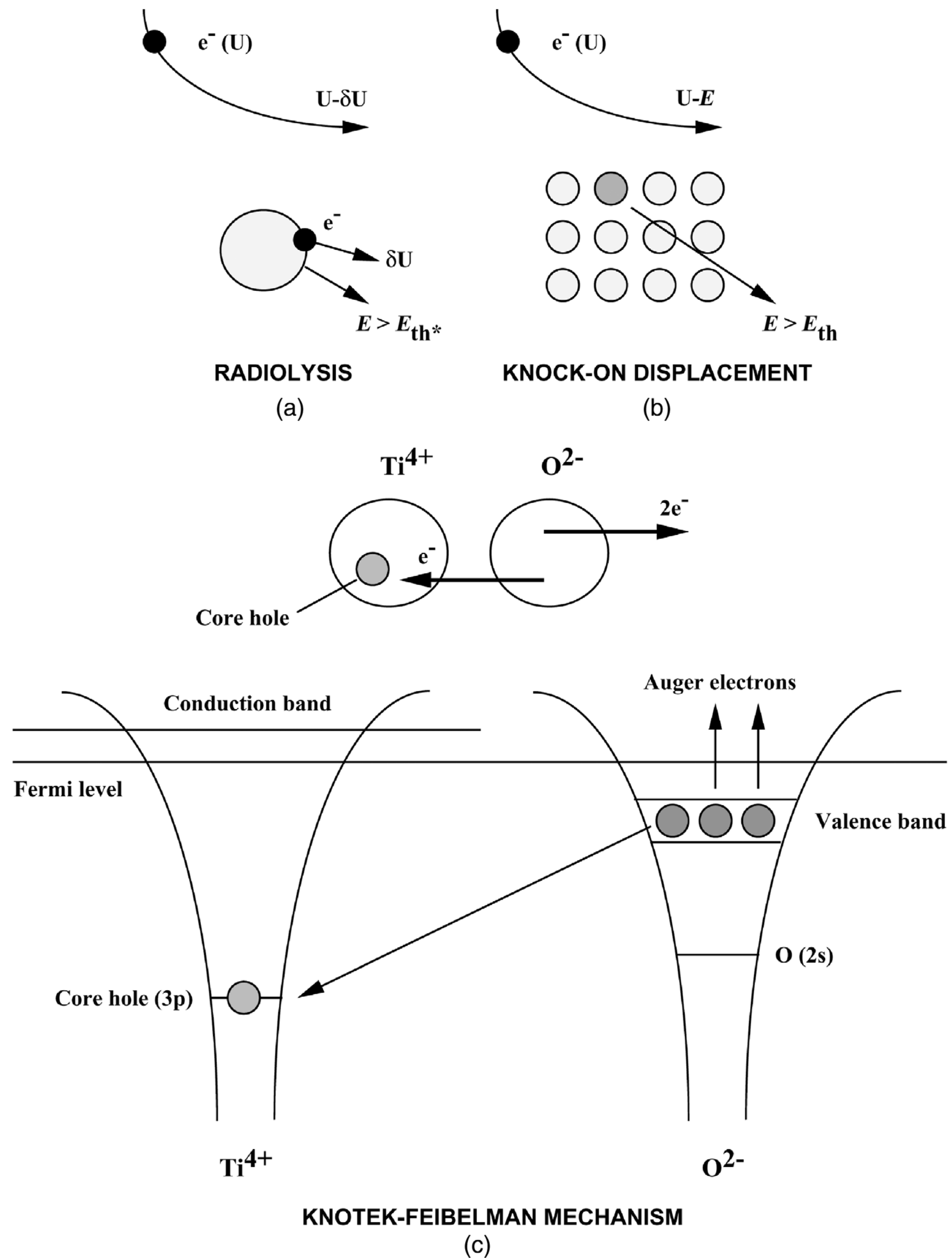

Fig. 2 Schematic of various mechanisms of permanent displacement of atoms under an electron beam. (a) Radiolysis and (b) knock-on displacement. E_{th} and E_{th*} are threshold energies for radiolysis and knock-on displacement, respectively. (c) Knotek–Feibelman mechanism. Here, the interatomic Auger decay of a maximal valency ionic solid (TiO_2) induces desorption. In Auger events, electrons are always removed from anion species resulting in highly repulsive final states and subsequent desorption.

of membrane–film substrate is not ideal for device fabrication due to its fragile nature. In contrast to using a dedicated STEM for lithography, both FEG-SEM and conventional electron beam lithography machine offer a more practical alternative for studying achievable resolution in resists and device fabrication on solid substrates. Amorphous oxides such as Fe_2O_3 and WO_3 deposited on silicon substrates were investigated for their suitability as electron beam resists as well as etch masks. In the case of Fe_2O_3, it undergoes amorphous to crystalline transition under an electron beam, which results in change in its solubility in HCl.[57] On the other hand, amorphous WO_3 films showed irradiation-induced chemical change and an amorphous to crystalline transition at lower and higher voltages, respectively, both affecting the change in

solubility of exposed region in basic solutions.[58,59] Although the dose requirement for exposure was lowered by some orders of magnitude, there was a noticeable increase in the LER due to the amorphous to crystalline transition.

2.2 *Inorganic Resists Based on Chalcogenide Glasses*

Concurrent to the investigation of metal halide and oxide-based inorganic resists, another resist platform had been simultaneously conceived utilizing chalcogenide glasses as resists materials. They typically comprise of sulfides and selenides of arsenic and germanium. Since the molecular network in chalcogenide glasses is much weaker compared to rigidly connected oxide glasses, exposure to various radiation sources such as ultraviolet/visible/infrared, x-rays, and electron beam can cause physiochemical alterations in chalcogenide glasses. Exploiting this phenomenon, chalcogenide glasses have been widely studied as lithographic resists.[60–62]

Perhaps the earliest report comes from Suhara et al. in 1975 who demonstrated electron beam-induced transformation in As-S chalcogenide glass leading to a visible change in the refractive index of the exposed area.[63] They further expanded the repertoire of resists to include evaporated As-S, As-Se-Ge, and As-Se-S-Ge chalcogenide systems. The electron beam-induced transformation was observed as change in the refractive index for doses as small as $\sim 1\ \mathrm{mC/cm^2}$.[63–66] The highlight of these earlier works is that they showed patterning using electron beam lithography can be carried out without development and etching steps. Interestingly, the patterned chalcogenide resist can be erased by heating and can be reused.[66] Subsequently, it was found that the chalcogenide films can elicit both positive- and negative-tone behavior depending on the choice of developer.[67,68] Exposed region of As-S-Se glass when subjected to an alkaline organic solution rendered it insoluble (negative tone) while As_2S_3 behaved as positive-tone resist for water-based NaOH solution. Further electron beam lithography studies with different compositions of As-S chalcogenide glass films using 30 kV electron beam, negative-tone high aspect ratio patterned structures down to 27 nm line widths with 7 nm spacing were fabricated using an amine-based alkaline developer.[69,70] Tanaka[71] reported that electrostatic force and electro-induced fluidity is the likely mechanism for the structural transformation. These chalcogenide glass films have been since used for fabricating gratings and optical diffractive elements.[72,73] Over the years, several alloyed compositions of As-Ge containing chalcogenide glasses, such as $As_{40}Se_{10}S_{40}Ge_{10}$,[64] $Ge_4As_4Se_{92}$,[74] $Ge_{30}As_4S_{66}$,[75] $Ge_9As_9Se_{82}$, and $Ge_{16}As_{24}Se_{60}$, have been studied for electron beam patterning.[76] In addition, negative-tone electron beam patterning has also been shown among chalcogenide glass compositions comprising of Ge-Sb-Se,[77] P-Ge-Se,[78] and Sb-Se.[79,80] While thermal evaporation has been the popular method for deposition of chalcogenide films, pulsed laser deposition has also been explored for maintaining stoichiometry of the complex compositions.[81]

Several reports have exploited electron beam-induced metal-doping mechanism for negative-tone patterning of chalcogenide resists, first reported by Yoshikawa et al.[82] A thin Ag film was deposited on top of the $Se_{85}Ge_{15}$ chalcogenide film by dipping into an aqueous $AgNO_3$ solution. On exposure by an electron beam, the diffusion of Ag into the chalcogenide film made the region insoluble in an alkaline solution. This approach features almost an order of magnitude-sensitivity improvement along with high patterning contrast ($\gamma \sim 8$). The approach was subsequently explored by varying the stoichiometric composition of the Ge-Se chalcogenide glass.[83–86] Similar patternability by Ag doping was also reported in GeS_2[87] and GeS_4 films.[88] On the other hand, Romero and Fitzgerald demonstrated that the $GeSe_2$ can be patterned using Cu thin film instead of Ag.[89] Similar Ag doping mechanism has also been reported for various compositions of As-S chalcogenide resists and resolution down to 30 nm was demonstrated.[90–93] Various compositions containing Sb_2S_3,[94] As_2Se_3,[92,94] and As-Ge-Se[95,96] have also been investigated for electron beam patterning using this approach.

2.3 *Spin-Coatable Metal-Containing Molecular Resists*

The fundamental fact is that inorganic resists based on metal halides and metal oxides are highly stable materials with strong ionic bonding and consequently require a high electron dose to make and/or break chemical bonds. In 1999, Saifullah et al. showed that instead of using a stable

inorganic resist to achieve high resolution, a relatively unstable metalorganic molecular material would potentially offer benefits such as a lower dose to exposure, simplified lithography by removing the lift-off step, and enabling much-desired single digit nanometer resolution.[97] From the same research group, a year earlier in 1998, Namatsu et al. reported breakthrough in patterning of inorganic materials—they demonstrated that hydrogen silsesquioxane (HSQ) could be patterned with both high resolution and sensitivity as well as with very low linewidth fluctuation.[98] These two reports broke the stalemate and provided the paradigm shift in direct patterning of functional materials by electron beam lithography.

2.3.1 *Spin-coatable metal oxide resists*

Stabilized metal alkoxide-based resists. Metal alkoxides are popular precursors for the development of electron beam-sensitive spin-coatable metal oxide resists. These are reactive compounds due to the presence of electronegative alkoxy groups, thus making the metal atom vulnerable to nucleophilic attack. Furthermore, alkoxides are highly unstable in an ambient atmosphere and susceptible to hydrolysis resulting in the formation of hydrated metal oxides alkoxides. This makes them unsuitable for handling in a lab atmosphere. However, their hydrolytic activity can be carefully tailored *via* chelation with β-diketones (e.g., acetylacetone, benzoylacetone) and β-ketoesters (e.g., methylacetoacetate, ethylacetoacetate). Both β-diketones and β-ketoesters undergo *keto-enol* tautomerism – the *enol* form is stabilized by chelation with metal alkoxides. This reduces the hydrolytic activity, most likely due to steric hindrance, and enables their handling under lab conditions. Due to high solubility of chelated metal alkoxides in organic solvents, this allows them to be spin-coated on a substrate in a conventional manner.

Aluminum *tert*-butoxide chelated with acetylacetone and ethylacetoacetate was the first metal alkoxide used as an electron beam-sensitive negative resist [Fig. 3(a)]. Chelation produced the gel that, when spin-coated on a substrate, gave Al_2O_3 resist.[97,103] Its sensitivity was $\sim$8 mC/cm^2 (at 80 kV) and exhibited $>10^6$ times more electron beam-sensitivity than sputtered amorphous Al_2O_3 resist films.[104] For the first time, the sensitivity of a metal oxide resist was demonstrated to be very close to the conventional electron beam resists such as calixarene and HSQ.[105,106] Furthermore, it was shown that the sensitivity of spin-coatable Al_2O_3 resist was tailorable depending upon the chelating agent that was employed to stabilize the alkoxide.[107] The weaker the ability of a chelating agent to bind with aluminum alkoxide, the higher is the electron beam sensitivity of the corresponding Al_2O_3 resist. Due to its small molecular size, Al_2O_3 resist showed single digit nanoscale resolution (8 nm) in the center of a 500 μm $\times$ 500 μm main field and $\sim$10 nm at its corners [Fig. 3(b)].[99] Since the lift-off step was absent, the patterned structure was mainly Al_2O_3, a functional material, which could be used as a mask to etch silicon.[103]

The chemistry of spin-coatable Al_2O_3 resist was used as a model to further develop resists of TiO_2,[100] ZrO_2,[101] HfO_2,[102] $PbTiO_3$, lead zirconium titanate (PZT), yttrium iron garnet (YIG), among others [Figs. 3(c)–3(f)].[108] Unsurprisingly, all these resists showed single digit nanometer resolution—out of which TiO_2 and ZrO_2 resists stand out for their low LER in sub-10 nm patterns and showed little deviation of the patterned structures from the designed widths. With further tweaking of sol–gel chemistry, resists for Al_2O_3,[109] TiO_2,[110] GeO_2,[111] PZT[112] among others were developed that are amenable to not only electron beam but also photon-based lithographies.[109] Both Al_2O_3 and TiO_2 resists used their respective alkoxides along with a phenylsilane to enable condensation of the inorganic network when exposed to an electron beam.[109,110] On the other hand, GeO_2 and PZT utilized their respective alkoxides with epoxy[111] and methacrylate groups,[112] respectively, to achieve patterning.

Electron beam patterning of a metal oxide using its respective metal alkoxide without a chelating agent is indeed possible but its deposition on a wafer is very cumbersome. Mitchell and Hu performed electron beam lithography on the condensed titanium *iso*-propoxide films to obtained TiO_2 patterns.[113–115] The deposition of titanium *iso*-propoxide required a high vacuum chamber and cooling of the wafer. Titanium *iso*-propoxide showed a high sensitivity to an electron beam, which is comparable to the conventional resists such as PMMA.

It was mentioned earlier that the chelation of metal alkoxides with β-diketones and β-ketoesters leads to the hydrolytic stability of spin-coatable metal oxide resists. With respect to

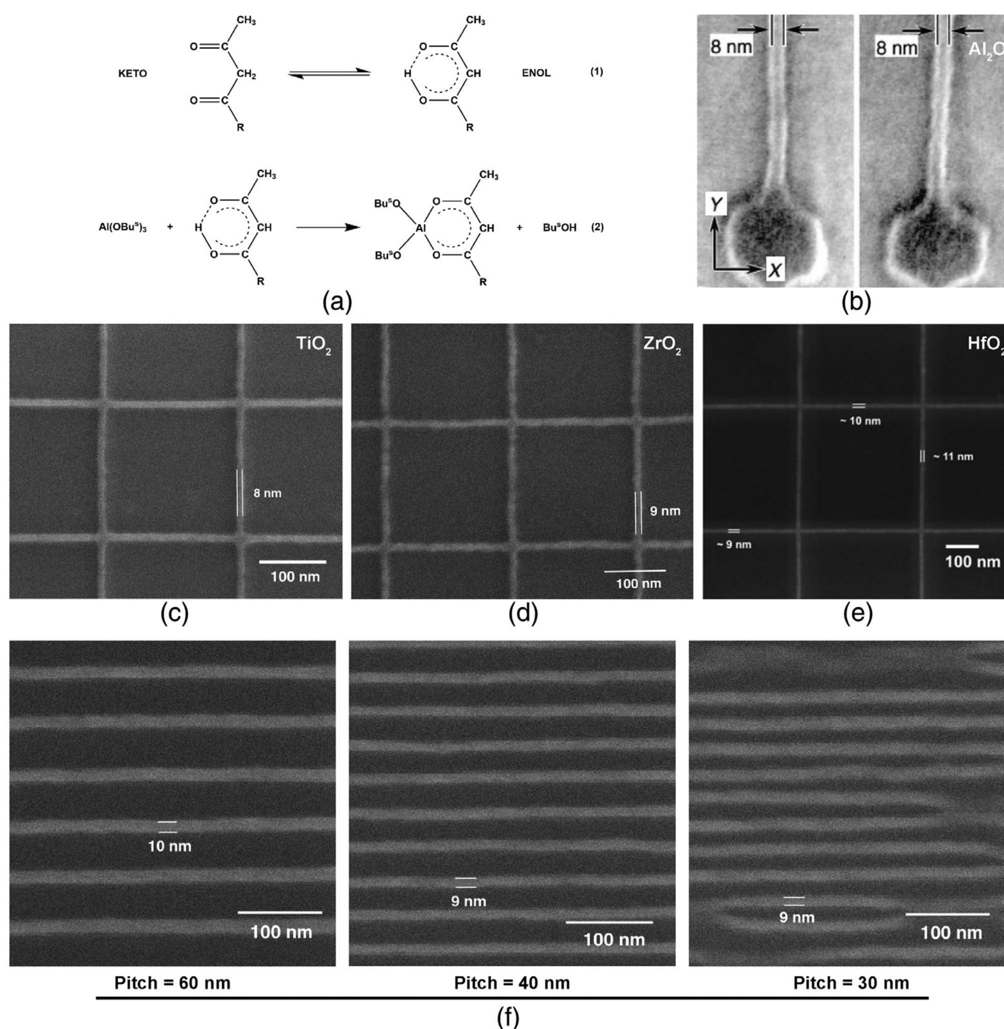

Fig. 3 Preparation and electron beam lithography of spin-coatable metal oxide resists. (a) Both β-diketones ($R = CH_3$ for acetylacetone) and β-ketoesters ($R = OC_2H_5$ for ethylacetoacetate) undergo *keto-enol* tautomerism and the *enol* form is stabilized by reaction with a metal alkoxide. As an example, aluminum tri-*sec*-butoxide, $Al(OBu^s)_3$, forms a bidentate molecular complex that is air stable and electron beam-sensitive. Single digit nanometer scale electron beam lithography of (b) Al_2O_3 (from Ref. 99), (c) TiO_2 (from Ref. 100), (d) ZrO_2 (from Ref. 101), and (e) HfO_2 using their respective resists (from Ref. 102). The resists from (c), (d) were prepared by reacting the respective alkoxides with benzoyl acetone. (f) Sub-10 nm dense features patterned using TiO_2 resist (from Ref. 100).

chemical bonding, the metal atom is bound to β-diketones and β-ketoesters in a bidentate fashion. When the resist is exposed to a beam of energetic electrons, the peaks associated with $\nu(C{=}O)$ and $\nu(C{=}C)$ vibrations in the chelate ring decrease in intensity with an increasing electron dose [Fig. 4(a)]. This suggests rapid radiolysis of the chelate ring, breakdown of the organic components, and their removal *via* the vacuum system of the electron beam writer [Fig. 4(b)]. In the FTIR spectra, with an increasing electron dose, this leads to bleaching of the bands associated with the original chelating organic molecules of the resist. The breakdown of organic components in the resist makes it insoluble in organic solvents such as alcohols and acetone, thus giving a negative-tone behavior.[103]

In the case of metal oxide resists where an alkoxide and a phenyl silane was used, exposure of the resist films to electrons and photons (UV or x-ray) result in degradation of the organic components and condensation of the inorganic network.[109,110] This process makes the exposed resist insoluble in organic solvents.

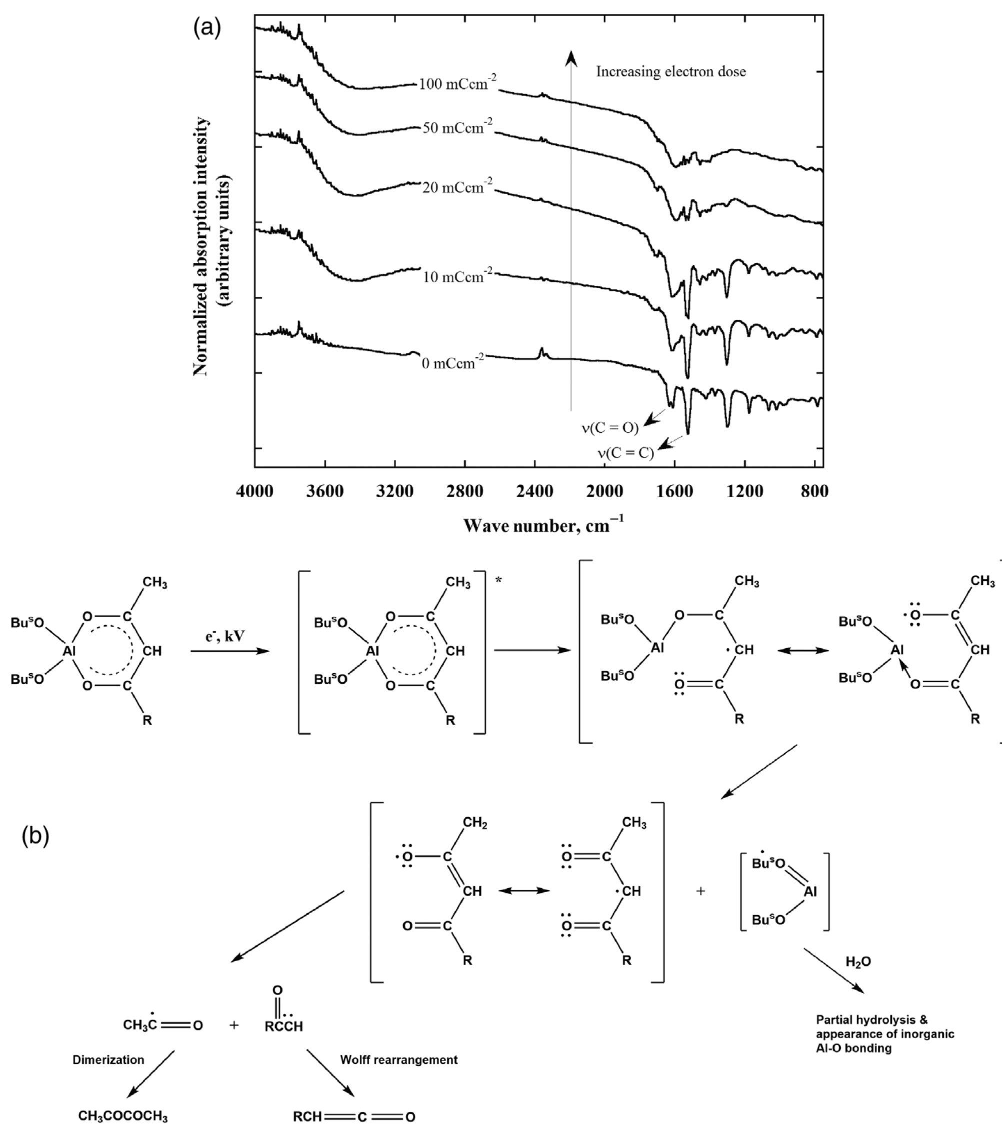

Fig. 4 (a) Electron beam exposure mechanism in spin-coatable Al_2O_3 resist. Exposure to a beam of energetic electrons result in the breakdown of chelate bonds that makes the resist insoluble in organic solvents such as acetone. (b) Proposed model of the exposure mechanism (from Ref. 103).

Metal carboxylate-based resists. Carboxylate salts of metals, especially metal naphthenates and neodecanoates (many of them popularly used as wood preservatives!), have been used as negative electron beam resists to pattern metal oxides *via* a post-heat treatment step. These are stable viscous liquids at room temperature. They are excellent candidates for high-resolution electron beam lithography. $YBa_2Cu_3O_7$ was the earliest oxide that was patterned using a mixture of metal naphthenates.[116] Several subsequent reports thereafter utilized submicron direct-write capabilities of metal naphthenates,[117] octylates,[118] and ethylhexanoates[119,120] to fabricated ferroelectric oxide patterns. Kiyohara et al. exploited the high etch resistance of the electron beam direct-write patterned metal octylates for pattern transfer into CVD diamond films.[121] Saifullah et al. showed that zinc naphthenate was capable of single digit nanometer resolution (7 nm) with an aspect ratio of ∼9 over the entire 500 μm × 500 μm main field [Fig 5(a)].[122,123] At 100 kV, zinc naphthenate showed a sensitivity of ∼15 mC/cm^2 and contrast of ∼3.3. These nanopatterns demonstrated very low LER ($3\sigma = 2.8$ nm). Heat-treatment of these patterns gave ∼5 nm wide ZnO lines [Fig. 5(b)]. Jones et al. fabricated nanoscale field-effect transistors of ZnO using a zinc neodecanoate resist.[124] Comparing zinc naphthenate and zinc

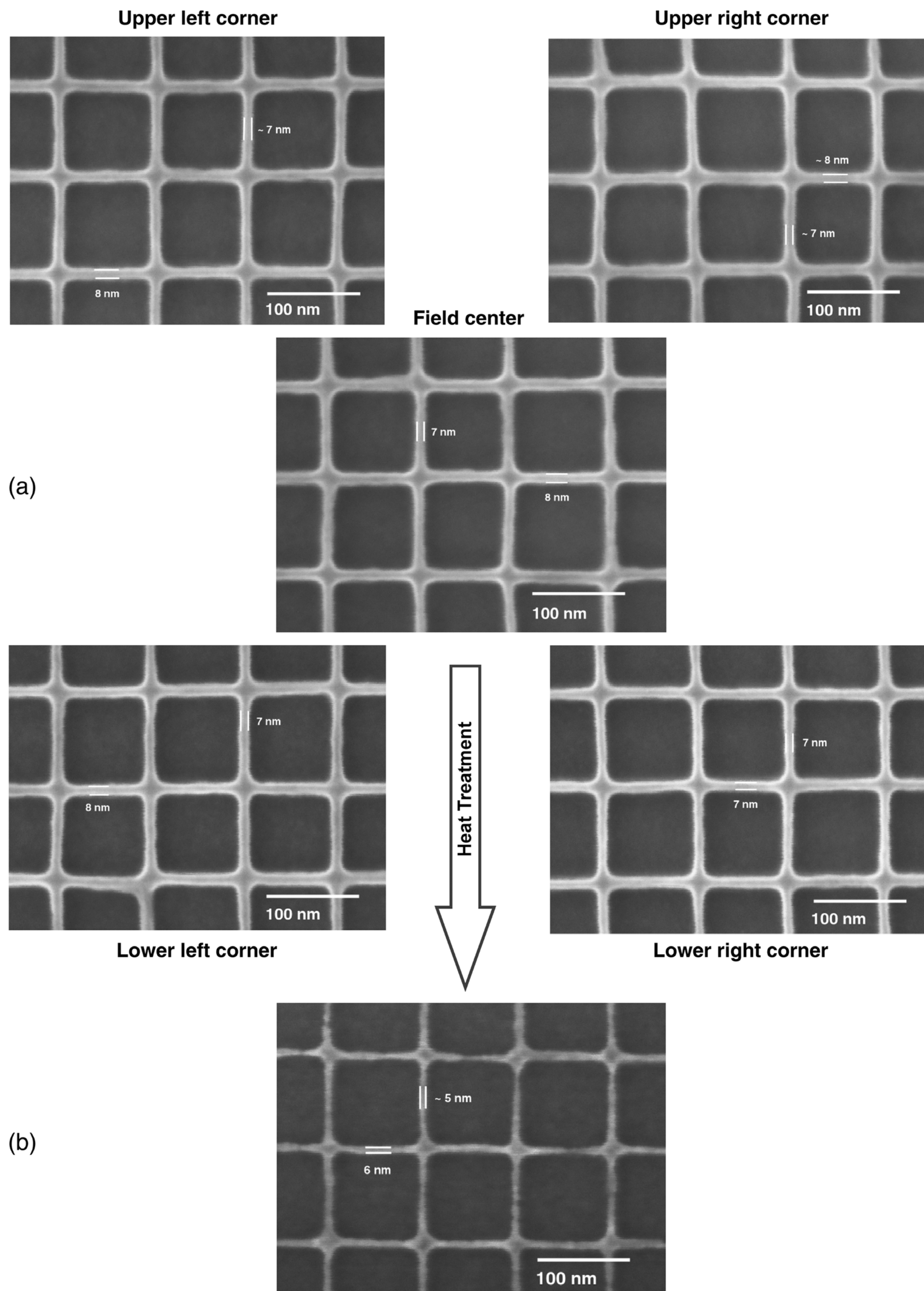

Fig. 5 (a) Electron beam lithography of zinc naphthenate resist showing sub-10 nm linewidths in the center as well as at the edges of the 500 μm $\times$ 500 μm main deflection field. The aspect ratio of these lines is ~9. A Leica VB6-UHR nanowriter was used to pattern them. These lines show an LER (3σ) of about 2.8 nm. This result demonstrates that with a right combination of patterning tool and resist, it is indeed possible to fabricate sub-10 nm features over the entire wafer. (b) Patterned resist was converted to ZnO by heat-treatment at 500°C for 1 h. The resulted in the reduction of linewidth to ~5 nm (from Ref. 122).

neodecanoate as resists for fabricating ZnO nanowires and FETs, Tiwale et al. demonstrated that both the precursors gave similar electronic properties.[125]

Electron beam lithography of iron naphthenate and the post-heat treatment of its patterns gave Fe_2O_3, which was used as a catalyst to grow carbon nanotubes.[126] Likewise, nickel and

copper naphthenates can also be patterned and heat-treated in air or a reducing atmosphere to give either their oxides or metals, respectively. Using the latter technique, Nedelcu et al. were able to obtain 8- and 4-nm wide lines of nickel and copper, respectively.[127] They also noted the low LER of the patterned structures. With the help of controlled annealing in pure hydrogen atmosphere, Bi et al. were able to achieve conversion of patterned copper naphthenate into graphene@copper composite.[128] Using condensed copper(II) pentafluoropropionate on a substrate, Berger et al. were able to pattern CuO, which on further annealing in a forming gas (5% H_2 in N_2) gave Cu structures.[129] Bhuvana et al. adopted a slightly different approach where they reacted palladium acetate with hexadecylthiol in an equimolar ratio to produce palladium acetate hexadecylthiolate. This behaved as a negative resist due to cross-linking of carbon chains when exposed to an electron beam. Heating the patterned resist at ∼240°C in air gave 30 nm wide lines of palladium metal.[130]

It was observed that reducing the size of the carboxylate group to an acetate led to the formation of metal oxide straightaway when the metal acetate was exposed to an electron beam. Stark et al. had initially reported patterning of palladium acetate by an electron beam exposure and subsequent development in chloroform. The solubility change due to exposure was attributed to the decomposition of palladium acetate leading to densification.[131] Chaker et al. sublimated zinc acetate onto a silicon substrate in vacuum. Exposing the thin film of zinc acetate to a beam of electrons led to the direct formation of 12-nm wide ZnO lines.[132] Similar electron beam exposure behavior was also observed for organotin acetate-based resists.[133]

Electron beam exposure study of a naphthenate resist using infrared absorption suggests cross-linking in the resist thus increasing the molecular weight and making it insoluble in organic solvents such as toluene. The result of this chemical transformation is negative-tone patterning.[117] It is believed that other metal carboxylates such as metal neodecanoates, octylates, ethylhexanoates, and palladium acetate hexadecylthiolate also undergo similar cross-linking to show negative-tone behavior. On the other hand, resists based on lower molecular weight carboxylate group such as zinc acetate undergo radiolysis leading to the removal of volatile organics and formation of ZnO under the beam.[132]

2.3.2 *Metal oxo-cage or oxo-cluster resists*

Among the conventional electron beam resists, HSQ has been extensively employed for high-resolution patterning.[98,106] This resist consists of an oxo-cluster of Si as its building block. Despite the issues with long-term stability, it possesses uniquely beneficial properties such as sub-10 nm resolution with extremely low LER and high etch resistance for pattern transfer thus proved to be a prelude to the development of spin-coatable metal oxide inorganic resists.

Perhaps the most significant development that followed was the resists based on aqueous chemistries of Zr and Hf.[134] These resists are based on solution processable $HafSO_x$ and $ZircSO_x$ amorphous films that can easily be deposited using aqueous solutions into smooth films. They were prepared by reacting aqueous solutions of $ZrOCl_2$ and $HfOCl_2$ with H_2O_2 and H_2SO_4. These resists show sensitivities as low as 8 $\mu C/cm^2$ at 30 kV electron beam exposure [Fig. 6(a)]—a significant achievement for a purely inorganic non-CAR. More importantly, they also showed lower values of line width roughness (LWR). The differential solubility between exposed and unexposed areas arises from electron beam-induced decomposition and elimination of peroxide, which promotes condensation reaction and crosslinking of metal-oxo bridges. In a subsequent report, 21-nm lines LWR as low as 1.6 to 1.8 nm was reported along with 18-nm half pitch patternability [Figs. 6(b) and 6(c)].[135] These encouraging results led to commercialization of the resist platform by Inpria Corp. They continued improvement of the resist processing reporting 12-nm half pitch patterning and across the board high dry-etch resistance compared to HSQ.[138] It has been further reported that $HafSO_x$ resist can be patterned down to 9 nm with 10-kV electron beam lithography [Fig. 6(d)].[136]

New developments in the field of metal-oxo cage resists are primarily driven by their success in EUV lithography, occasionally with a comparative study involving electron beam patterning. Inpria Corp. introduced a next generation of metal oxide inorganic resists based on tin (Sn) in an attempt to improve their absorbance for EUV radiation.[139] This development further spurred a slew of organotin-based resists. While Sn dodecamer (Sn_{12})-based resist chemistry attracted

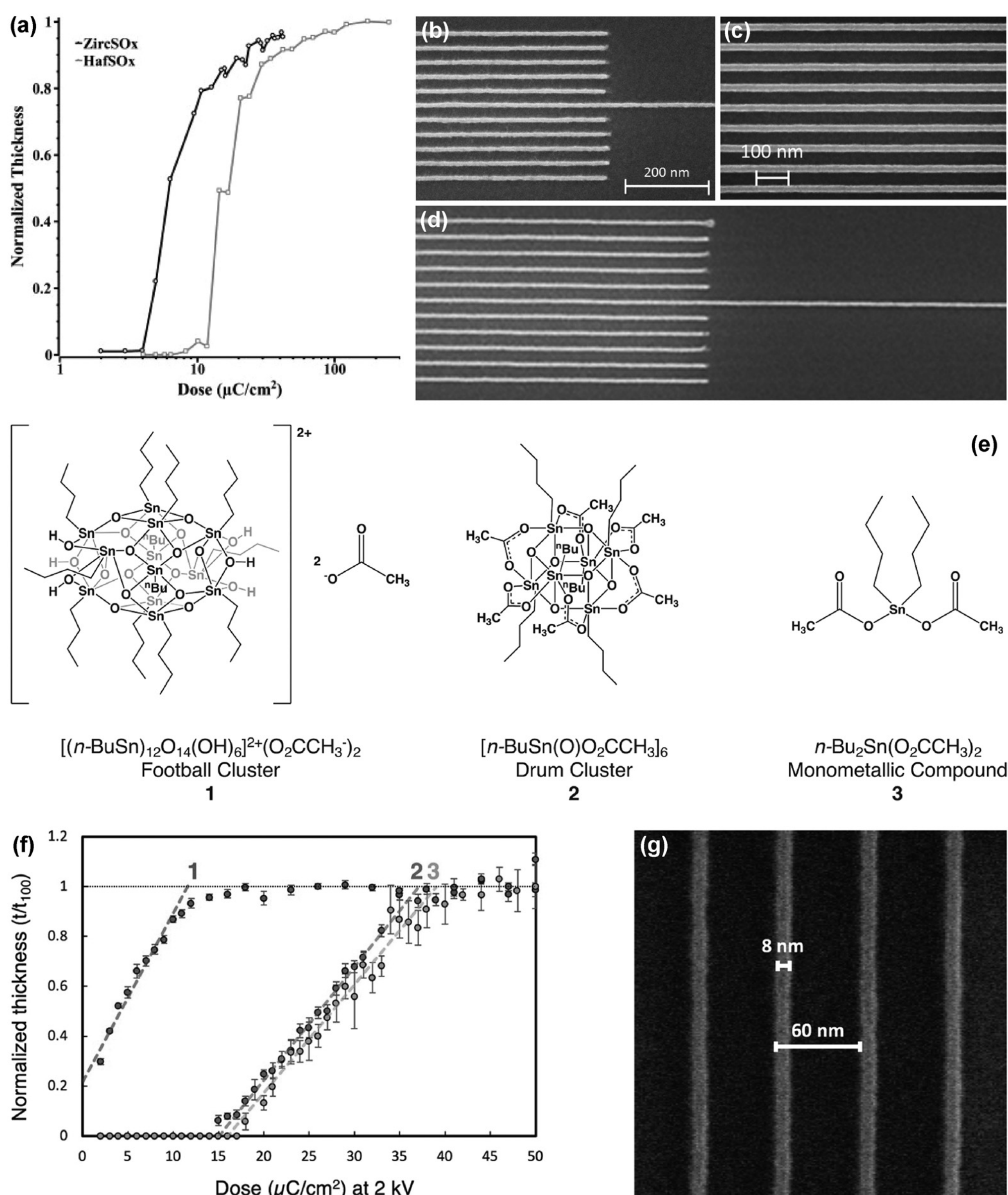

Fig. 6 Electron beam patterning of metal sulfoxide resists at 30 kV. (a) Exposure response curves for $ZircSO_x$ and $HafSO_x$ with metal-to-sulfate ratios of 1:0.5 and 1:0.55, respectively, after development in 25% w/w TMAH (from Ref. 134). (b) 18 nm LS patterns after 244 $\mu C/cm^2$ exposure and (c) 21 nm lines on 60 nm pitch showing LWR of 1.6 to 1.8 nm after 436 $\mu C/cm^2$ exposure (from Ref. 135). (d) 9 nm lines spaced at 35 nm patterned in HafSOx resist using 10 kV electron beam (from Ref. 136). (e) Molecular structures of organotin carboxylate resists and (f) their dose response curve when exposed with a 2 kV electron beam (from Ref. 133). (g) High-resolution patterns of dodecameric organotin resist patterned using 400 $\mu C/cm^2$ exposure using a 30-kV electron beam and developed in 2-heptanone (from Ref. 137).

particular attention,[140] other chemistries, such as sodium-centered butyltin (β-$NaSn_{13}$),[141] butyltin oxo hydroxo cluster,[142] and hexameric organotin carboxylates,[133] are interesting as well [Figs. 6(e) and 6(f)]. During the patterning of these resist materials, radiolysis of the Sn–C bond initiates hydrolysis and condensation reactions giving rise to tin oxide framework that is rendered less soluble in a developer. It has also been suggested that post-exposure bake may cause dehydration along with crosslinking of organic ligands, which may impact the solubility contrast. Resolution down to ~8 nm linewidth has been thus demonstrated using Sn-based chemistries [Fig. 6(g)].[137] Oxo-cluster-based resists containing different metals such as Ti, Zr, Hf, Zn and the effect of ligand chemistry on EUV lithography performance is being actively

investigated.[143–147] In a recent study, oxo-cluster resist based on Ni has also shown ∼9 nm resolution isolated features with LER as low as ∼1.8 nm patterned using electron beam lithography.[148]

2.3.3 *Spin-coatable metal sulfide resists*

This is a recent addition in the armory of metal-containing molecular resists for electron beam lithography to obtain directly metal sulfide under an electron beam. An earlier attempt involved electron beam lithography of palladium hexadecylthiolate, a negative-tone resist, which was converted to Pd_4S *via* a post-thermolysis step.[149]

We mentioned in the section "Stabilized metal alkoxide-based resists" that metal alkoxides are nucleophiles that can be stabilized *via* chelation. One of the other ways to stabilize a metal alkoxide, $[M^+(OR)^-]$, is to insert a mild electrophile such as carbon disulfide (CS_2). This leads to the formation of a metal xanthate or metal dithiocarbonate, $M^+(ROCS_2)^-$ (where R is the alkyl group), which is just about stable at room temperature. Metal xanthates rapidly undergo decomposition when heated around 100°C, some even at a lower temperature. Furthermore, many of them freely dissolve in organic solvents such as chloroform. Their borderline stability and good solubility in organic solvents make them highly suitable candidates as electron beam resists.

Transition metal xanthates are conveniently prepared by metathesis reaction between a metal salt and potassium alkylxanthates in an aqueous medium. They usually exhibit bidentate bonding between the transition metal atom and the two sulfur atoms of xanthate group, which can be potentially cleaved using an energetic beam of electrons [Fig. 7(a)]. In an early report, mixture of metal xanthates was used as precursor for direct-nanopatterning copper indium sulfide for use in hybrid photovoltaics with EUV interference lithography.[153] The work of Saifullah et al. is the earliest demonstration of direct patterning of metal sulfide under an electron beam. They showed the suitability of zinc alkylxanthate-based spin-coatable resists for direct lithography of ZnS.[150] The dose sensitivity and solubility of zinc alkylxanthates increases with increasing length of the alkyl chain. The sensitivity of these resists was close to 35 mC/cm^2 at 100 kV and were capable of achieving very high resolution – ZnS lines as small as 6- and 10-nm dots with pitches as close as 22 nm were achieved [Figs. 7(b) and 7(c)]. Just like spin-coatable metal oxides, the lift-off step was noticeably absent here as well. Fabricated patterns of ZnS showed defect-induced photoluminescence related to sub-band-gap optical transitions [Figs. 7(d) and 7(e)]. Similarly, Recatala-Gomez et al. employed bismuth(III) ethylxanthate to pattern bismuth sulfide (Bi_2S_3) to study its thermoelectric properties [Fig. 7(f)].[151]

For direct patterning of MoS_2, tetranuclear molybdenum thiocubane ($Mo_4S_4{}^{6+}$) complexes with xanthate ligands were used.[152] They were prepared by refluxing molybdenum hexacarbonyl with different dialkylxanthogen disulfides in toluene. These complexes [$Mo_4S_4(ROCS_2)_6$, where R is an alkyl group] show excellent solubility in organic solvents and show good film formability. Their electron beam sensitivity is very close to that of ZnS resist and are capable of single digit nanometer resolution. An electron-beam-induced radiolysis of a molybdenum thiocubane resist resulted in the fabrication of 9-nm-wide MoS_2 lines and dense dots as small as 13 nm with a pitch of 33 nm [Fig. 7(g)].

To pattern metal sulfides using an electron beam, Wang et al. used a different precursor based on metal alkylthiocarbamate.[154] They reacted butyldithiocarbamic acid with transition metal oxides to form metal butyldithiocarbamates. These compounds were chemically transformed to metal sulfides *via* patterning using electrons/photons followed by a heat-treatment step. For electron beam writing, unlike the xanthates, the dose required for butyldithiocarbamates was enormously high—7200 mC/cm^2 for Sb_2S_3, 3600 mC/cm^2 for ZnS, and 4800 mC/cm^2 for PbS. This is not surprising as metal alkyldithiocarbamates, in contrast to metal alkyldithiocarbonates (or xanthates), are quite stable compounds. More stability of the precursor translates into higher dose requirement to chemically change the material, with a requirement of post-heat-treatment step to remove residual organics. Micro-Raman and micro-FTIR spectroscopies were used to follow time-resolved electron beam damage studies in metal sulfide resists based on metal xanthates. These studies suggest that exposure to a beam of electrons lead to quick

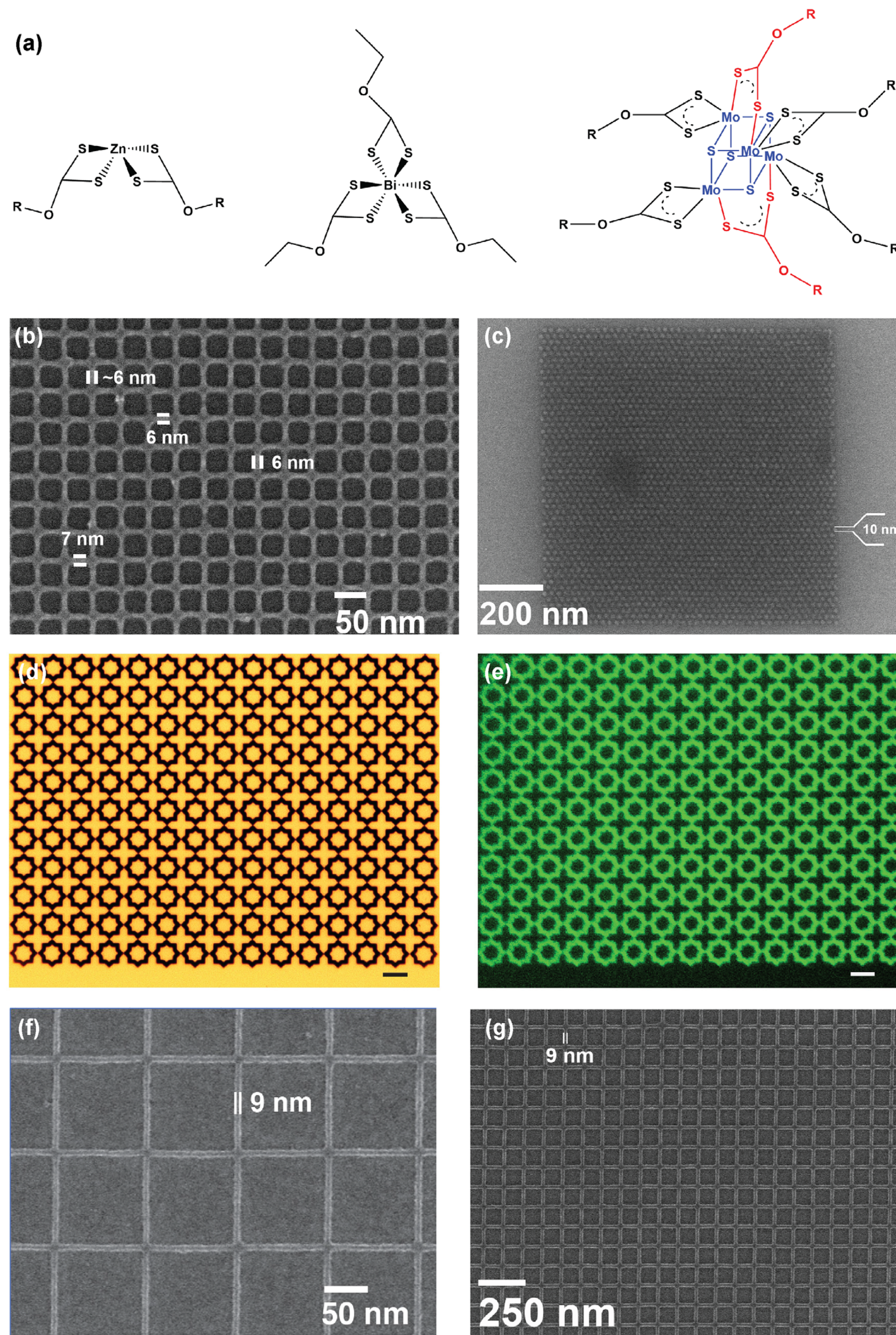

Fig. 7 (a) Molecular structure of zinc alkylxanthate (left), bismuth ethylxanthate (middle), and molybdenum thiocubane (right), where R- indicates the alkyl group. Molybdenum thiocubanes have the formula $Mo_4S_4(ROCS_2)_6$. Here in the central cube, molybdenum and sulfur ions occupy diagonally opposite corners as shown in blue. Shown in black are four xanthate groups that are coordinated to a molybdenum ion in a chelating bidendate fashion. Two xanthate groups in red are coordinated to a molybdenum ion in a bridging bidendate manner. (b) Electron beam lithography of zinc butylxanthate gives 6 nm wide lines and (c) 10 nm dots with 22 nm pitch of ZnS (from Ref. 150). (d) Optical and (e) confocal images of patterned structures showing defect-induced photoluminescence from ZnS nanocrystals when imaged between 500 and 600 nm wavelength range (scale bar = 10 μm). (f) Direct patterning of Bi_2S_3 (from Ref. 151), and (g) MoS_2 at single digit nanometer scale using electron beam lithography (from Ref. 152).

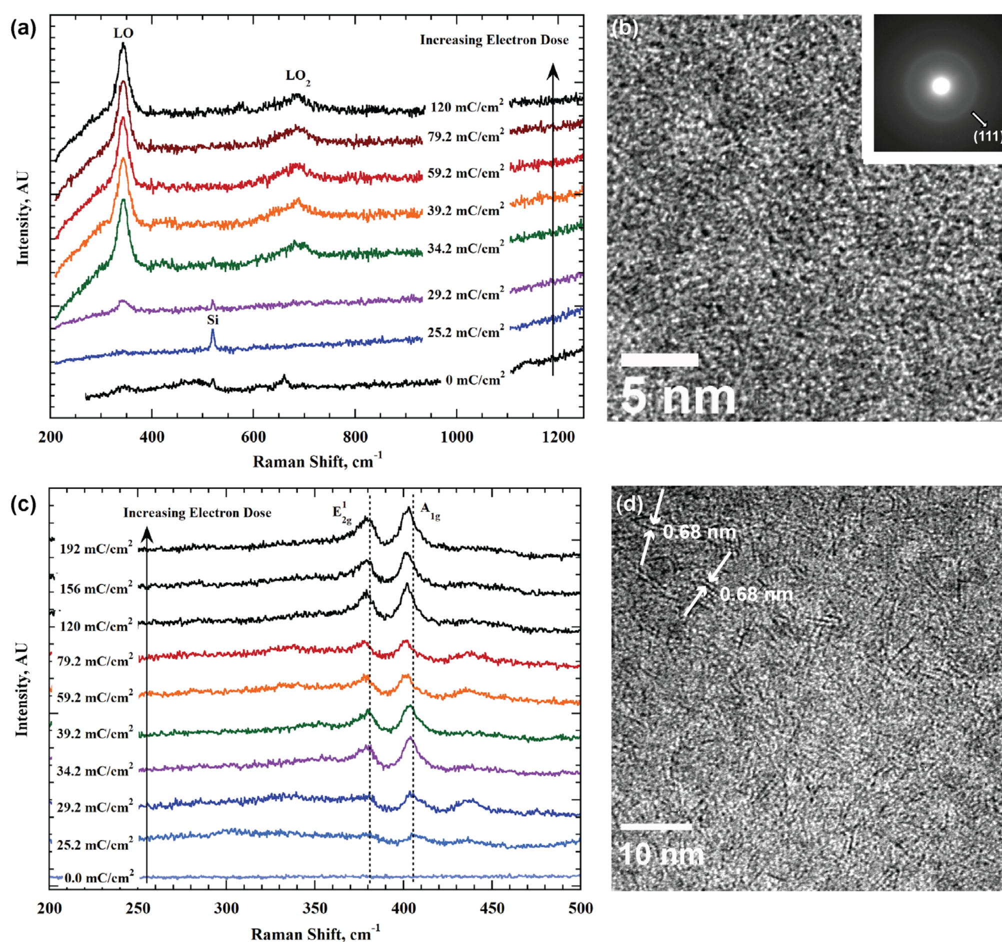

Fig. 8 (a) Evolution of Raman spectra of ZnS resist with increasing electron dose. It is characterized by the appearance and increase in intensity of first- and second-order longitudinal optical phonon (LO and LO_2, respectively) modes. (b) The corresponding TEM image shows the *in situ* formation of cubic ZnS nanocrystallites (from Ref. 150). (c) Evolution of Raman spectra of MoS_2 resist with increasing electron dose showing the appearance of characteristic E^1_{2g} and A_{1g} peaks. (d) The TEM image shows lattice fringes that are spaced at 0.68 nm that corresponds to the d-spacing of (002) crystal planes in MoS_2 (from Ref. 152).

disappearance of xanthate moieties, most probably *via* the Chugaev elimination with the concurrent formation of metal sulfide [Fig. 8].[150–152] This phenomenon makes the exposed resist insoluble in organic solvents and gives rise to the negative-tone behavior.

2.4 *Spin-Coatable Metal-Containing Nonmolecular Resists*

Being nonmolecular, this class of resist offers considerable freedom in the way a metal is incorporated in the resist. The purpose of the addition of metal is to improve the resist performance and to provide certain functionality to the patterned material. Macroscopically, resists in this class fall into two categories—resists having a polymer backbone and organic ligand capped nanoparticles. On one hand, metal salts or metallic nanoparticles are added to organic polymer to improve its patterning performance; on the other hand, metallopolymers themselves have been explored for nanolithography. Interestingly, nanoparticle formulations have sometimes been exploited for direct-writing of functional nanostructures such as conducting nanowires and light-emitting quantum dots. The solubility switch mechanism exploited among these nanoparticle resists at times can simply be radiation-induced decomposition of the organic ligands causing the nanoparticles to condense into rigid inorganic structures. However, in some cases, elegant ligand exchange reaction takes place when exposed to radiation, changing their solubility in

specific solvents. An overview of some of these nonmolecular resists reported over the years is provided in this section.

2.4.1 *Metal-containing polymeric resists*

Polymeric resists such as PMMA are widely used in electron beam lithography. To improve their properties and to serve a functional purpose, metallic species are added to them. Dating back to 1979, Webb and Hatzakis reported that copolymers of methyl methacrylate and metal methacrylates exhibit improvement of sensitivity and contrast for electron beam lithography when optimal metal content is incorporated into the composition.[155] They observed that the sensitivity of the resist improved with increase in the atomic number of the incorporated metal. In 1986, direct writing of gold nanostructures using electron beam exposure was demonstrated using gold containing organometallic polymer.[156]

Chuang et al. used an interesting approach where they induced oxidation–reduction reaction with an electron beam (at a dose of $<2\ \mathrm{mC/cm^2}$) in a lanthanum strontium manganese oxide (LSMO) gel that had polyvinyl alcohol as fuel and nitrate ions (NO_3^-) as an oxidant.[157,158] Lanthanum, strontium, and manganese nitrates provided NO_3^- ions in the gel. This type of autoignition process is characterized by a sharp and an intense exotherm and is a selfpropagating combustion reaction. Spin-coatable and water-soluble LSMO gel is a dual tone resist whose behavior can be modified by changing the dose. Further reports demonstrate that if Ag or Au salts are added to polyvinyl alcohol, electron beam exposure can induce acid catalyzed crosslinking within polyvinyl alcohol rendering the exposed regions insoluble in water thus exhibiting negative-tone behavior.[159,160] The addition of silver nitrate to poly(vinyl pyrrolidone) also exhibited negative-tone pattern ability; however, it was found that the nanocomposite formulation showed lower patterning resolution.[161] Better results were obtained for a negative resist that consists of chloroauric acid ($HAuCl_4$) and poly(vinyl pyrrolidone) hybrid, giving a minimum Au feature size of ∼100 nm after electron beam lithography.[162]

In a recent report, the addition of ∼2-nm-sized Ag nanoparticles to *tert*-butyl 2-ethyl-6-(4-hydroxyphenyl)-4-phenylheptanoate (Terpolymer) resist served as radiation sensitizer. Incremental addition of Ag nanoparticles up to 1 wt. % exhibited 10-fold sensitivity improvement with acetonitrile as developer.[163] The resist composition also showed ∼12 nm resolution with ∼1.5 nm LER. Zong et al. reported doping commercial electron beam resists with bimetallic (PtFe, PtCo, etc.) nanoparticles leading to significant improvement in their mechanical properties.[164] The modified resist exhibited increased pattern collapse mitigation and enhanced etch resistance for pattern transfer using ion-beam etching. Con et al. used coevaporation of Cr and polystyrene to incorporate metal into the polymeric matrix and reported stark improvement in the patterning contrast as well as dry etch resistance.[165] The authors were thus able to fabricate 100-nm Si-nanopillars with an aspect ratio as high as 35 using ∼90-nm thick resist.

Several metallopolymers have been utilized for electron beam patterning. Earliest of the reports out of the Bell Labs utilized ferrocene containing polymers such as poly(vinyl ferrocene) for negative-tone electron beam resists.[166,167] One such platform utilized polyferrocenylsilane (PFS) backbone synthesized by ring opening polymerization of silaferrocenophanes.[168] Clendenning et al. demonstrated direct writing of magneto-optically active ceramics using cobalt-clusterized PFS.[169] This approach was further extended to PFS resists containing Ni and Mo clusters as pendent moieties.[170] In another report, metallopolymer with iron and phosphorus containing backbone, PFpP, was used for negative-tone electron beam patterning.[171] Features as small as 17 nm were obtained [Figs. 9(a) and 9(b)]. Use of water-soluble poly(sodium 4-styrenesulfonate) (PSS) as a negative-tone electron beam resist was also reported having sensitivity in the similar range as PFS and PFpP.[173]

2.4.2 *Ligand capped nanoparticle resists*

In the earliest of the reports, sub-50-nm direct electron beam patterning was demonstrated using surfactant stabilized Pd, Pd/Pt,[174,175] and Au cluster.[176–179] Electrically active nanowire structures were also demonstrated by direct electron beam lithography on a Ru cluster polymer.[180]

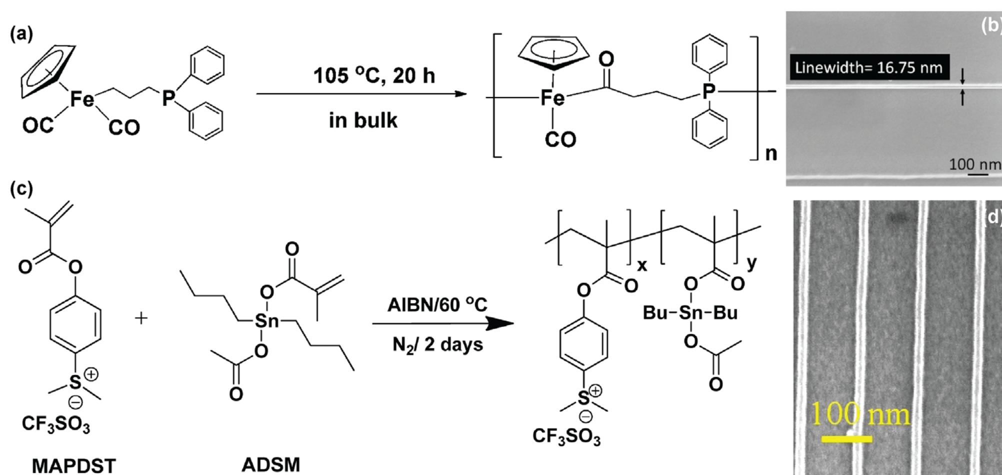

Fig. 9 (a) Migration insertion polymerization synthesis of PFpP resist. (b) High resolution isolated line features of PFpP resist fabricated by 15 nC/cm exposure using 20 kV electron beam (from Ref. 171). (c) Sn containing PBP resist is synthesized by free radical copolymerization of (4-(methacryloyloxy)phenyl)-dimethylsulfoniumtriflate (MAPDST) and ADSM. (d) 12.3 nm wide line patterns of the Sn containing PBP resist exposed with 400 $\mu C/cm^2$ with 20 kV electron beam and developed in 0.002 N TMAH (from Ref. 172).

Langmuir–Blodgett films of alkanethiol-capped gold nanoparticles were also subjected to electron beam exposure to define nanowire structures at doses as low as 0.5 mC/cm^2, much lower than previous reports that used passivated gold nanoclusters.[181]

ZrO_2 and HfO_2 nanoparticles with various acrylic acid ligands were investigated for their application in nanolithography by Ober's group at Cornell University. A systematic study with different developer solutions led to the fabrication of resist patterns down to ~32 nm with ketone-based solvent developers.[182] The approach was further extended to resist formulations containing ZnO_x, TiO_x, InO_x and SnO_x; with optimization of resist processing, 15-nm half pitch patterns were achieved.[183] However, the patterned features suffered from high LER along with significant residual scum artifact that could be the consequence of nanoparticle size and high concentration of photoacid generator (PAG).

One of the widely known classes of functional nanoparticles is that of colloidal quantum dots owing to their tunable narrow bandwidth photoluminescence. However, their integration into scalable device platform is challenging since they can lose their performance when agglomerated. Few recent studies have utilized electron beam exposure as a means to directly pattern quantum dots into high-resolution optoelectronic devices. Nandwana et al. demonstrated electron beam direct patterning of trioctylphosphine oxide functionalized CdSe/ZnS quantum dots, where electron beam-induced crosslinking of the ligands rendered exposed regions insoluble in toluene.[184] Subsequently, CdSe/CdS quantum dot patterns down to 30-nm lines and 50-nm disks were also reported.[185] Wang et al. demonstrated a versatile approach for direct-patterning of quantum dots by exploring a range of different ligand chemistries. They were able to show CeO_2 nanoparticle patterns down to 30 nm linewidth, whereas CdSe quantum dot patterns down to 70 nm linewidth were also reported.[186] More recently, direct patterning of quantum dots using an electron beam as well as EUV exposure has also been reported.[187] Here upon exposure, oleic acid, the capping ligand for quantum dots, and a carboxylic acid, underwent cross-linking, rendering the exposed area insoluble in an apolar developer. Electron-beam-induced cross-linking of long-chain ligands (carboxylate and oleylamine) was also utilized for direct patterning of $CsPbBr_3$ nanocrystals.[188] This type of cross-linking is similar to what has been observed earlier in metal carboxylate-based resists (see section "Metal carboxylate-based resists").

2.4.3 *Metal-containing polymer-bound PAG resists*

CARs have been load-bearers for semiconductor high volume manufacturing for decades due to their fast photo-speed, largely owing to highly radiation-sensitive small molecule additive called

the PAG. However, as the critical dimension started to drastically decrease, PAG aggregation and acid diffusion posed a pertinent challenge for pattern fidelity. One of the solutions that was implemented was PAG grafting into the backbone of the copolymeric resists namely—polymer-bound PAG (PBP) resists.[189,190] However, with the emergence of EUV lithography, these primarily organic compositions started falling short of achieving adequate radiation absorption and promoting the incorporation of inorganic/metal species into the resist mixture.

A PBP composition containing ferrocene pendent group was reported to exhibit improved electron beam sensitivity and resolution compared to the composition without ferrocene group.[191,192] A resist concept using W and Mo polyoxometalates as pendent group in PBP composition has also been explored.[193] A recent report detailed doping of PBP resist with thiolated Ag nanoparticles that demonstrated improved sensitivity to electrons and lower LER for sub-15 nm features.[194] The performance improvement was attributed to the photomultiplication effect induced by the Ag nanoparticles supporting plasmonic resonance. Similarly, copolymer synthesized using acetyldibutylstannyl methacrylate (ADSM) for incorporating Sn containing pendent group was also demonstrated, providing resolution down to ∼12.3 nm with LER < 1.3 nm [Figs. 9(c) and 9(d)] after development in 0.002 N tetramethylammonium hydroxide (TMAH).[172]

2.5 *Emerging Metal Containing Resist Platforms*

2.5.1 *Metal-organic framework-based resists*

Metal-organic frameworks (MOF) are organic–inorganic hybrid crystalline porous compounds that consist of metal ions coordinated to organic ligands to form one-, two-, or three-dimensional cage-like structures. These materials can be deposited with high degree of regularity leading to highly regular absorbance. The use of zeolitic imidazolate framework particles loaded into phenyltriethoxysilane sol–gel matrix was reported for generating negative-tone patterns using deep x-ray exposure.[195] MOF inspired Zn-cluster resist was also demonstrated to pattern dense negative-tone structures of 25-nm half pitch with electron beam lithography and 13-nm half pitch with EUV exposure.[196] Recently, Tu et al. demonstrated direct patterning of MOFs using electron beam and x-ray lithographies.[197] Direct patterning avoids damage due to etching and leaves the porosity and crystallinity of the patterned MOF intact. Unlike the previous reports, positive-tone resist behavior was observed here due to the crystalline to amorphous transition of exposed regions becoming soluble in solvent such as dimethyl sulfoxide. They were able to pattern sub-50 nm features of MOFs with potential applications in high-performance dielectrics, and selective and sensitive sensors.

2.5.2 *Infiltration synthesis of hybrid resists*

Vapor phase infiltration synthesis: an *ex-situ* approach for converting a conventional polymeric resist into a hybrid resist was recently demonstrated.[198,199] Infiltration synthesis approach is based on vapor phase precursors typically used for atomic layer deposition (ALD); however, contrary to adsorption driven thin film deposition, precursors are made to diffuse into polymeric resist where they bind to reactive functional groups within the polymer. As a result, metal oxide moieties are grown inside the resist matrix. In the initial report, PMMA resist was converted into PMMA-AlO_x and its performance for electron beam lithography was studied. With an increasing amount of infiltration, the resist exhibited decrease in sensitivity while improving the patterning contrast by sixfold. At the same time, stark improvement in the dry etching resistance was observed giving Si etch selectivity estimated to be in excess of 300. Patterned features with ∼30 nm linewidth were transferred in an Si substrate to fabricate Si fins with an aspect ratio of ∼17. Subsequently, an approach for improving the resist sensitivity by Hf-infiltration has also been introduced.[200] In a recent report, infiltration of various metal oxides into a high sensitivity resist was reported with a resolution ∼30 nm.[201] While controllability and ease of implementation being the high points, further maturation of this resist platform is required.

Table 1 provides a succinct summary of electron beam lithography of metal-containing resists reported over the years.

Table 1 Summary of key metal-containing resists reported over the years.

Resist category	Material	Development	Resist tone	Sensitivity	Resolution	Year	Ref.
Self-developing metal halides	NaCl	Self-develop	Positive	0.1 C/m^2 at 100 kV	8 nm lines, 5 nm holes	1978	21
	NaCl	Self-develop	Positive	100 C/m^2 at 100 kV	1.5 nm lines, 2 nm holes	1981	22
	AlF_3	Self-develop	Positive	20 C/cm^2 at 100 kV	20 nm lines	1986	24
		H_2O	Negative	3 C/cm^2 at 100 kV	20 nm lines		
Self-developing metal oxides	β-alumina	Self-develop	Positive	$\sim 2 \times 10^7$ C/cm^2 at 100 kV	2 nm lines, 2 nm holes	1983	35
Chalcogenide glass	Arsenic sulfide	Alkaline amine solvent	Negative	10 nm/cm at 30 kV	30 nm lines spaced at 15 nm	2006	69
Metal alkoxide-based	Aluminum tri-*sec*-butoxide + ethyl acetoacetate	Acetone	Negative	4 mC/cm^2 at 80 kV	8 nm lines	1999	97,99
Metal carboxylate-based	Zinc naphthenate	Toluene	Negative	15 mC/cm^2 at 100 kV	7 nm lines	2005	122,123
Metal oxo-cage or oxo-cluster	$HafSO_x$ and $ZircSO_x$	25% TMAH	Negative	8 $\mu C/cm^2$ at 30 kV	15 nm lines	2009	134
	$HafSO_x$	25% TMAH	Negative	50 $\mu C/cm^2$ at 10 kV	9 nm lines spaced at 35 nm	2016	136
Metal sulfides	Zinc butylxanthate	Chloroform	Negative	46 mC/cm^2 at 100 kV	6 nm lines, 10 nm dots	2017	150
Metal-containing polymers	Ag nanoparticles in terpolymer	Acetonitrile	Negative	50 $\mu C/cm^2$ at 20 kV	12 nm	2020	163
	PFpP	Tetrahydrofuran	Negative	12 mC/cm^2 at 20 kV	17 nm	2015	171
Ligand capped nanoparticles	ZrO_2 NPs with methacrylic acid ligands + PAG	Alcohol	Negative	10 $\mu C/cm^2$ at 100 kV	32 nm	2013	182
Metal-containing polymer bound PAG	MAPDST-co-ADSM	0.002 N TMAH	Negative	80 $\mu C/cm^2$ at 20 kV	~12.3 nm	2020	172

3 Perspectives for EUV Lithography

Electron beam and EUV lithographies share certain common concerns while their evolution has been largely pivoted on serving different end-users. The former has been primarily used for research prototyping while the latter has commercial interests in mind. On the other hand, both lithographic techniques have vested interests in the continuation of the Moore's Law in some form or another. Innovations in semiconductor industry are going to continue with research-based lithography technologies leading and providing new paths or templates for commercial lithography to emulate—a good case in point being the advent of HSQ and spin-coatable metal oxide resists developed for electron beam lithography that were once scientific curiosities in nanofabrication are now being used as a template for spin-coatable metal-containing resist development in EUV lithography. Although sufficient progress has been made in the recent years, we believe that the full spectrum advantage of metal-containing resists in EUV lithography remains untapped. Electron beam lithography, on the other hand, has already benefitted from these; it is incumbent upon the EUV lithography to exploit these prevalent knowhows.

There is, however, a caveat to the mechanics of energy transfer to the resist during electron beam exposure compared to EUV exposure. As mentioned earlier, EUV radiation ionizes the resist by majorly exciting electrons from deep-valence or shallow-core levels and produces secondary electrons that subsequently cause the chemical-solubility change.[14] On the other hand, during the electron-beam exposure, electrons transfer merely a tiny fraction of the incident energy to the resist before reaching the substrate and mainly excites valence electrons. A fraction of the electrons that reach the substrate is backscattered over a range of several microns causing a substantial proximity effect that adds a background exposure contribution of ~5% to 10% and the energy transported by backscattering can be up to 75% of the energy delivered by forward scattering.[15] During the EUV exposure, the trajectory range of the generated photoelectrons would be around ~25 nm as per a Monte-Carlo simulation conducted on PMMA.[202] Moreover, mean energy amounting to ~35 eV is lost by the electrons in the resist where electron-beam exposure of several keV is typically used. This excess energy is delivered to the substrate that may cause localized heating. While on an average ~35 eV energy is lost by electrons during EUV exposure as well, the energy delivered by a photon is only 92 eV, leading to only small amount of energy transferred to the substrate. Thus, substrate heating issue is unlikely to be present during EUV lithography.[15]

3.1 *Molecular Resists for High Patterning Resolution*

Using a 0.5-nm probe in a VG HB5 STEM, the demonstration of 2-nm diameter holes and 1.5-wide troughs in thin NaCl films by Isaacson and Muray has been an important achievement in electron beam lithography.[22] It sets out an important principle that a combination of ultrafine beam and a lower molecular weight resist is the key to achieving very high patterning resolution, in principle very close to the diameter of the beam. In fact, much of the early work on electron beam "machining" of metal halides and metal oxides quite consistently showed single digit nanometer patterning. Given that the modern commercial electron beam writers have a beam diameter of 2 to 5 nm, it is expected that they should be able to achieve sub-10 nm patterning. This is indeed so—single digit nanoscale lithography is now routinely possible with spin-coatable metal oxide and metal sulfide molecular resists based on metalorganic materials. Can patterning resolution close to the diameter of electron probe even be possible? Recently, using a small molecular weight spin-coatable CdS resist, Saifullah et al. demonstrated that patterning resolution close to the size of electron probe is possible in a commercial electron beam writer.[203] With a ~3.7-nm diameter electron beam, they were able to fabricate 4-nm wide CdS lines over a 5 μm × 5 μm area. This result suggests that with a suitable combination of resist chemistry and patterning instrument, lithography can be pushed down to an angstrom-scale.

There is a growing realization among the practitioners of EUV lithography that smaller molecular weight metal-containing resists are key to attaining not only finer resolution but also to achieve lower values of LWR. Molecular organometallic resist for EUV (MORE) platform now consists of close to 70 different resist platforms from 10 different metals.[204] This platform exploits high sensitivity of Sb metal and various carboxylate chelating groups.[205,206] Indeed,

it was observed from contrast curves that the photosensitivity of the resist is directly dependent on molecular weight of the carboxylate group.[206,207] In a later study of complexes containing Pt and Pd, interestingly, oxalate complexes exhibited positive-tone behaviors while carbonate complexes gave negative-tone patterns.[208]

3.2 *Mitigation of Stochastic Variations in Patterned Features*

Every part of the lithography process suffers from stochastic variability. When the feature sizes are large, then the number of events being averaged in various steps in lithography is sufficiently high, and in this case the stochastic nature of the lithography process can be safely ignored. However, as the feature sizes reduce in size, the scale over which the average behavior is observed also shrinks. The outcome of this is the increasing importance (and dominance) of stochastic variability in lithography. The consequence of this is the LER where a standard deviation of the edge position could be a few nanometers. In feature sizes greater >100 nm, such small amounts of variation could easily be ignored. However, in sub-20 nm lithography, and more so in single digit nanoscale patterning, even a single nanometer of uncertainty in the edge position becomes a matter of considerable significance.

The sources of stochastic variation in the lithography can originate from both the exposure process and the resist materials. Electron beam lithography being a serial process, the exposure is carried out as discrete beam-shots at specified pitch, which can result in substantial LER and/or pattern broadening if the latter is not properly controlled. Although during EUV lithography, the stepper exposes the entire pattern simultaneously, the spatial variation among EUV photons has much more prominent effect compared with earlier lithography wavelengths. The energy possessed by individual EUV photons (92 eV) is much higher than the ArF wavelength (6.4 eV). Consequently, for a given exposure dose, a much smaller number of EUV photons are absorbed by fixed volume of a photoresist, making the stochastic variability (also called as photon shot noise) in their position a much larger concern.[209] Given that the photon shot noise limits the minimum possible LER, resist possessing high optical absorption and quantum efficiency are essential.[210] On the resist side, compositional inhomogeneity is the root cause of manifestation of stochastic phenomenon. Variability in the length of the polymer chains and their spatial distribution can have significant impact on the pattern fidelity. In the multicomponent systems, such as CARs, the issue is further exacerbated by the distribution of the PAG molecules and their agglomeration along with the variation in generation and diffusion of the photoacid.[11] While many resist studies to date report patterning results with electron beam as well as EUV lithography, a direct comparison of their LER implications is in fact not straightforward due to the mechanistic differences in the resist exposure. In an attempt to explore the significance of absorption shot noise on LER, a study systematically normalized the absorption, point spread function, and process latitude and discovered slightly larger mean LER for electron beam lithography compared to EUV lithography in the case of two commercial CARs tested.[15] More such studies are called for to better elucidate the critical sources of LER manifestation.

Small molecule metal-containing resists used in electron beam lithography do not suffer from intermolecular chain entanglement like polymer resists that can lead to internal stresses and pattern distortion. The smaller unit size of these molecular resists also leads to much more close-packed and uniform distribution of the units, compared to larger radii of gyration for polymeric resists. Moreover, being non-CARs, they do not suffer from acid-diffusion induced LER either. Instead, in many cases, the exposure induced radiolysis of molecular resists leads to outgassing of volatile byproducts accompanied by condensation of the metal containing units that are insoluble in developer. In some instances, such as metal sulfide and zinc acetate resists, the exposed regions become fully inorganic, where surface energy minimization and Ostwald ripening leads to relatively smoother pattern edges. Collectively, these small molecule metal-containing resists are likely to have profound impact on minimizing stochastic-induced pattern roughness.

3.3 *Simplification of Lithography Process*

Typically, solution synthesized resist materials—polymeric, nanoparticle/nanocluster-based—have inherent size distribution of their building units. As the semiconductor industry heads into

smaller technology nodes, these size variations can contribute substantially to the LWR. Moreover, during wet development, pattern collapse associated with high aspect ratio structures due to capillary forces poses substantial challenge for achieving higher resolution features. Recently, Lam Research Corp. has introduced a complete dry-processing concept for EUV lithography to address the issue of pattern collapse and LWR.[211] This approach is pivoted on deposition of inorganic resist films conformally using ALD and post-exposure development to be carried out using reactive ion etching-based plasma chemistry. High-density 9-nm half pitch features with < 3 nm LWR have been reported with this approach.

It is possible to envision even simpler process flow, where the development step itself can be avoided. As we noted earlier, an advantage of inorganic resists, chiefly metal halides and metal oxides, is that they are "self-developing" and thus needed little or no chemical development post-exposure. The concept of "self-development" in electron beam lithography, although not a great practical success, resulted in the removal of development step, thereby simplifying the lithography process and avoided the pitfalls associated with pattern collapse during wet development. Early reports on "self-developing" electron beam resists have elucidated benefits of resist compositions that generate vapor phase byproducts on exposure to radiation. Such an approach may well help in further performance improvement of EUV resists. A lesson to be learnt from the evolution of electron beam lithography resists is that the key to realizing self/dry-developing resists lies in synthesizing resist compositions that are just stable enough at room temperature, such that little to no post-exposure bake would lead to patterned resist structures.

Another simplification of the lithography process is the removal of lift-off or pattern transfer step. The introduction of spin-coatable metal oxide and metal sulfide resists led to direct patterning of functional materials without the need for lift-off or etch step. It shortened the process of obtaining the patterned material, as the resist itself served as its source. Furthermore, this resulted in tighter control of critical dimensions and enabled access to single digit nanoscale resolution, which is otherwise very challenging using a conventional method of lift-off. In the case of EUV lithography, with the advent of metal-containing resists, there are already efforts to simplify the patterning process, that is, to use the patterned resist itself as an etch mask or simply as a dense insulating oxide layer.[139]

The higher mechanical robustness of the metal-containing resists presents yet another process simplification potential. As it is, metal-containing resists are less prone to capillary force-induced pattern collapse compared to the conventional organic resists. Moreover, conventionally, stack of layers such as spin-on-carbon, spin-on-glass, etc., have been inherent part of semiconductor processing. While such layer stack has been helpful in achieving optimal etch selectivity to realize required high aspect ratio pattern transfer, the corresponding process flow thus requires multiple etch steps, which by itself may affect the overall throughput, but more importantly it can cumulatively also exacerbate occurrence of defects and LER/LWR. Metal-containing resists, owing to their improved etch robustness, can alleviate the need for such complex etch-stack, further simplifying the patterning process. An effective example maybe of the infiltration synthesized hybrid resist that has demonstrated up to ∼60 times improved etch selectivity.[198,199]

3.4 *Direct Writing of Functional Materials*

The flexibility in the choice of metal-containing molecular resist materials in electron beam lithography has led to the emergence of direct patterning of many functional materials at a single digit nanoscale resolution. Their patterning at such a high resolution *via* the traditional process of exposure, development, and lift-off/etch would have been extremely challenging if not impossible. As we have already seen, currently many metals, metal oxides, and metal sulfides can be directly patterned. In future, a host of metal chalcogenides could be potentially added to this list. A number of reports have already demonstrated application of such directly written functional materials in various device platforms with performance at par with the state of the art. A few examples to note would be ZnO nanowire transistors,[122,124] substoichiometric Bi_2S_3-based thermoelectric device,[151] and photovoltaics.[153] With the increasing interest in the heterogeneous integration and on-chip functionalities (such as on-chip memory), direct writing of functional materials using EUV lithography can have lasting impact in shaping the next generation of technology.

3.5 *Positive-Tone Patterning for Contacts Holes*

Most of the metal-containing resist development in EUV lithography has primarily been focused on negative-tone patterning, whereas positive resist development has been relatively limited. Particularly for features such as contact holes and vias, positive-tone development is highly advantageous over negative resists since patterning dense contact hole array with negative-tone resist either requires tremendously high exposure dose or two line-space exposures perpendicular to each other.[212] However, to pattern dense contact holes with positive tone, CARs are still the material of choice.[213] Electron beam lithography has previously demonstrated positive tone patternability of self-developing inorganic resists down to 2 nm holes[22] as well as chain-scission PMMA resist with 1 nm holes patterning.[214] Further development is clearly required to develop metal-containing resist chemistries capable of patterning such high-resolution positive-tone patterns at much higher photo-speed. Synthesis of room-temperature metastable compositions, which can be converted to less stable moieties on exposure, may benefit in overcoming this impediment to aggressively scaling down contact hole/via patterning.

4 Conclusions

We have presented a thorough overview of the vast portfolio of metal-containing resist explored by electron beam lithography. During the initial period evaporated inorganic resists exhibiting high resolution were studied albeit they required extremely high exposure dose. Over the period, spin-coatable metal-containing molecular resists with relatively higher sensitivity were developed that consistently demonstrated single digit nanometer patternability and low LER. The advent of HSQ resist opened up a paradigm of oxo-hydroxo linked metal oxide cage/cluster resists that became one of the earliest generations of hybrid resists that were implemented for EUV lithography. Simultaneously, a number of nonmolecular resist approaches have also been explored spanning across metal salts/nanoparticles addition to polymeric backbone resists, metallopolymers, organic ligand-capped nanoparticle resists as well as metal-containing polymer-bound-PAG resists. While some of these approaches have been translated to EUV lithography, others can provide a useful pathway to overcome number of persistent challenges as the semiconductor industry aims to move into high-NA EUV lithography ecosystem in the coming years.

Acknowledgments

The work discussed in this review was performed at various places, *viz*., University of Cambridge (Department of Materials Science and Metallurgy and the Nanoscience Centre), NTT Basic Research Laboratories, Atsugi-shi (Japan), and the Institute of Materials Research and Engineering (Singapore). MSMS acknowledges the help and advice of Professor Colin J. Humphreys, Dr. Kenji Kurihara, Dr. Kenji Yamazaki, Dr. Hideo Namatsu, Dr. Toru Yamaguchi, Professor Sir Mark Welland, Professor Dae-Joon Kang, Dr. David Hasko, Professor Wilhelm Huck, Professor Ullrich Steiner, Dr. Mohamed Asbahi, Professor K. R. V. Subramanian, Dr. Sudhiranjan Tripathy, Professor Kedar Hippalgaonkar, and Professor Suresh Valiyaveettil. This research used the resources of the Center for Functional Nanomaterials (CFN), which is a U.S. Department of Energy Office of Science User Facility, at Brookhaven National Laboratory (BNL) under Contract No. DE-SC0012704. NT would also like to acknowledge guidance and discussions with Dr. Chang-Yong Nam and Professor Sir Mark Welland, along with Dr. Aaron Stein, Dr. Yury Alaverdyan, and Dr. Atif Aziz. The authors have no competing interests to declare.

References

1. E. Buitrago et al., "Chapter 4: EUV lithography process challenges," in *Frontiers of Nanoscience*, A. Robinson and R. Lawson, Eds., Vol. 11, pp. 135–176, Elsevier, Amsterdam (2016).
2. P. Naulleau, "Chapter 5: EUV lithography patterning challenges," in *Frontiers of Nanoscience*, A. Robinson and R. Lawson, Eds., Vol. 11, pp. 177–192, Elsevier, Amsterdam (2016).

3. D. L. Goldfarb et al., "EUV chemically amplified resist component distribution and efficiency for stochastic defect control," *Proc. SPIE* **11326**, 1132609 (2020).
4. T. Tsuchimura, "Recent progress in photo-acid generators for advanced photopolymer materials," *J. Photopolym. Sci. Technol.* **33**, 15–26 (2020).
5. T. Allenet et al., "Progress in EUV resist screening by interference lithography for high-NA lithography," *Proc. SPIE* **11854**, 118540N (2021).
6. T. Nishikubo and H. Kudo, "Recent development in molecular resists for extreme ultraviolet lithography," *J. Photopolym. Sci. Technol.* **24**, 9–18 (2011).
7. T. Itani and T. Kozawa, "Resist materials and processes for extreme ultraviolet lithography," *Jpn. J. Appl. Phys.* **52**, 010002 (2013).
8. P. D. Ashby et al., "Resist materials for extreme ultraviolet lithography: toward low-cost single-digit-nanometer patterning," *Adv. Mater.* **27**, 5813–5819 (2015).
9. S. Ghosh et al., "Recent advances in non-chemically amplified photoresists for next generation IC technology," *RSC Adv.* **6**, 74462 (2016).
10. D. de Simone, Y. Vesters, and G. Vandenberghe, "Photoresists in extreme ultraviolet lithography (EUVL)," *Adv. Opt. Technol.* **6**, 163–172 (2017).
11. L. Li et al., "Extreme ultraviolet resist materials for sub-7 nm patterning," *Chem. Soc. Rev.* **46**, 4855–4866 (2017).
12. T. Manouras and P. Argitis, "High sensitivity resists for EUV lithography: a review of material design strategies and performance results," *Nanomaterials* **10**, 1593 (2020).
13. C. Luo et al., "Review of recent advances in inorganic photoresists," *RSC Adv.* **10**, 8385–8395 (2020).
14. K. D. Closser et al., "The importance of inner-shell electronic structure for enhancing the EUV absorption of photoresist materials," *J. Chem. Phys.* **146**, 164106 (2017).
15. S. Bhattarai, A. R. Neureuther, and P. P. Naulleau, "Study of shot noise in photoresists for extreme ultraviolet lithography through comparative analysis of line edge roughness in electron beam and extreme ultraviolet lithography," *J. Vac. Sci. Technol. B* **35**, 061602 (2017).
16. D. F. Ogletree, "Chapter 2: Molecular excitation and relaxation of extreme ultraviolet lithography photoresists," in *Frontiers of Nanoscience*, A. Robinson and R. Lawson, Eds., Vol. **11**, pp. 91–113, Elsevier, Amsterdam (2016).
17. I. Haller, M. Hatzakis, and R. Srinivasan, "High-resolution positive resists for electron-beam exposure," *IBM J. Res. Dev.* **12**, 251–256 (1968).
18. E. G. Lean and A. N. Broers, "Microwave surface acoustic delay lines," *Microwave J.* **13**, 97–101 (1970).
19. A. N. Broers et al., "Electron beam fabrication of 80 Å metal structure," *Appl. Phys. Lett.* **29**, 596–598 (1976).
20. A. N. Broers, J. M. E. Harper, and W. W. Molzers, "250-Å linewidths with PMMA electron resist," *Appl. Phys. Lett.* **33**, 392–394 (1978).
21. A. N. Broers et al., "High resolution electron beam fabrication using STEM," in *Proc. 9th Int. Congr. Electron Microsc.*, Toronto, Ontario, J. M. Sturgess, Ed., Vol. 3, pp. 343–354 (1978).
22. M. Isaacson and A. Muray, "*In situ* vaporization of very low molecular weight resists using ½ nm diameter electron beams," *J. Vac. Sci. Technol. B* **19**, 1117–1120 (1981).
23. A. Muray, M. Isaacson, and I. Adesida, "AlF_3–a new very high resolution electron beam resist," *Appl. Phys. Lett.* **45**, 589–591 (1984).
24. E. Kratschmer and M. Isaacson, "Nanostructure fabrication in metals, insulators, and semiconductors using self-developing metal inorganic resist," *J. Vac. Sci. Technol. B* **4**, 361–364 (1986).
25. M. S. M. Saifullah et al., "Electron beam nanolithography of iron(III) fluoride using a scanning transmission electron microscope," *Inst. Phys. Conf. Ser.* **147**, 325–328 (1995).
26. C. J. Humphreys et al., "Electron beam nano-etching in oxides, fluorides, metals and semiconductors," *Scanning Microsc. Suppl.* **4**, 185–192 (1990).
27. E. Kratschmer and M. Isaacson, "Progress in self-developing metal fluoride resists," *J. Vac. Sci. Technol. B* **5**, 369–373 (1987).
28. A. Scherer and H. G. Craighead, "Barium fluoride and strontium fluoride negative electron beam resists," *J. Vac. Sci. Technol. B* **5**, 374–378 (1987).

29. A. Scherer et al., "Fluoride etch masks for high-resolution pattern transfer," *J. Vac. Sci. Technol. B* **8**, 28–32 (1990).
30. P. M. Mankiewich et al., "High resolution electron beam lithography on CaF_2," *Appl. Phys. Lett.* **44**, 468–469 (1984).
31. R. Zanetti et al., "The effect of grain size on electron beam hole drilling in CaF_2," *Inst. Phys. Conf. Ser.* **138**, 67–70 (1993).
32. W. Langheinrich and H. Beneking, "Fabrication of metallic structures in the 10 nm region using an inorganic electron beam resist," *Jpn. J. Appl. Phys.* **32**, 6218–6223 (1993).
33. J. Fujita et al., "Sub-10 nm lithography and development properties of inorganic resist by scanning electron beam," *Appl. Phys. Lett.* **66**, 3065–3067 (1995).
34. J. Fujita et al., "Sub-10 nm lithography and development properties of inorganic resist by scanning electron beams," *J. Vac. Sci. Technol. B* **13**, 2757–2761 (1995).
35. M. E. Mochel et al., "Electron beam writing on a 20-Å scale in metal β-aluminas," *Appl. Phys. Lett.* **42**, 392–394 (1983).
36. S. D. Berger et al., "Electron energy-loss spectroscopy studies of nanometer-scale structures in alumina produced by intense electron-beam radiation," *Philos. Mag. B* **55**, 341–358 (1987).
37. R. W. Devenish et al., "Nanolithography using field emission and conventional thermionic electron sources," *Ultramicroscopy* **28**, 324–329 (1989).
38. I. G. Salisbury et al., "Nanometer scale electron beam lithography in inorganic materials," *Appl. Phys. Lett.* **45**, 1289–1291 (1984).
39. J. L. Hollenbach and R. C. Buchanan, "Oxide thin films for nanometer scale electron beam lithography," *J. Mater. Res.* **5**, 1058–1072 (1990).
40. C. J. Morgan et al., "Electron beam nanolithography of sputtered amorphous Al_2O_3 and the proximity effect," *Inst. Phys. Conf. Ser.* **119**, 503–506 (1991).
41. C. J. Morgan et al., "Ultimate limits of lithography," *Phys. World* **5**(11), 28–32 (1992).
42. P. S. Turner et al., "Nanometre hole formation in MgO using electron beams," *Philos. Mag. Lett.* **61**, 181–193 (1990).
43. R. W. Devenish et al., "Electron-beam machining of MgO and ZnO in the STEM," *Inst. Phys. Conf. Ser.* **98**, 215–218 (1990).
44. S. D. Berger, J. M. Macaulay, and L. M. Brown, "Radiation damage in TiO_x at high current density," *Philos. Mag. Lett.* **56**, 179–185 (1987).
45. M. S. M. Saifullah et al., "Electron beam damage in titanium dioxide films," *Inst. Phys. Conf. Ser.* **153**, 167–170 (1997).
46. G. S. Chen, C. B. Boothroyd, and C. J. Humphreys, "Novel fabrication method for nanometer-scale silicon dots and wires," *Appl. Phys. Lett.* **62**, 1949–1951 (1993).
47. M. S. M. Saifullah et al., "Electron energy loss spectroscopy of silicon nanostructures in a scanning transmission electron microscope," in *Electron Microsc. 96 (Committee of Eur. Soc. Microsc., Brussels)*, Vol. 2, pp. 123–125 (1998).
48. J. Fujita et al., "Nanostructure fabrication using the selective thermal desorption of SiO_2 induced by electrons," *Appl. Phys. Lett.* **69**, 638–640 (1996).
49. A. J. Pauza et al., "Direct writing of weak links in high T_c superconductors with electrons," in *Proc. Third Int. Supercond. Electron. Conf.*, University of Strathclyde, Glasgow (Scotland) and Meeting Makers, Glasgow, pp. 352–355 (1991).
50. M. S. M. Saifullah et al., "Irradiation damage of inorganic resists on a silicon substrate," in *"The Electron" Proc. Int. Cent. Symp. the Electron*, A. Kirkland and P. D. Brown, Eds., IOM Communication Ltd., London, pp. 531–537 (1998).
51. L. W. Hobbs, "Radiation effects in analysis of inorganic specimens by TEM," in *Analytic Electron Microscopy*, J. J. Hren, J. I. Goldstein, and D. C. Joy, Eds., pp. 437–480, Plenum Press, New York (1980).
52. D. Pooley, "F-centre production in alkali halides by electron-hole recombination and a subsequent [110] replacement sequence: a discussion of the electron-hole recombination," *Proc. Phys. Soc. (Lond.)* **87**, 245–256 (1966).
53. N. Kabler and R. T. Williams, "Vacancy-interstitial pair production via electron-hole recombination in halide crystals," *Phys. Rev. B* **18**, 1948–1960 (1978).

54. M. L. Knotek and P. J. Feibelman, "Ion desorption by core-hole auger decay," *Phys. Rev. Letts.* **40**, 964–967 (1978).
55. M. L. Knotek and P. J. Feibelman, "Stability of ionically bonded surfaces in ionizing environments," *Surf. Sci.* **90**, 78–90 (1979).
56. R. P. Feynman. "There's plenty of room at the bottom," in *Miniaturisation*, H. D. Gilbert, Ed., pp. 282–296, Chapman and Hall, London and New York (1960).
57. G. W. Kammlott and W. R. Sinclair, "Fe_2O_3 – an inorganic electron resist material," *J. Electrochem. Soc.* **121**, 929–932 (1974).
58. M. Baba and T. Ikeda, "A new inorganic electron resist using amorphous WO_3 film," *Jpn. J. Appl. Phys.* **20**, L149–L152 (1981).
59. F. Carcenac et al., "High voltage electron beam nanolithography on WO_3," *J. Vac. Sci. Technol. B* **14**, 4283–4287 (1996).
60. H. Jain and M. Vlcek, "Glasses for lithography," *J. Non-Cryst. Solids* **354**, 1401–1406 (2008).
61. V. Lyubin, "Chalcogenide glassy photoresists: history of development, properties, and applications," *Phys. Status Solidi B* **246**, 1758–1767 (2009).
62. H. Jain, A. Kovalskiy, and M. Vlcek, "17–Chalcogenide glass resists for lithography," in *Chalcogenide Glasses Preparation, Properties and Applications*, J.-L. Adam and X. Zhang, Eds., pp. 562–596, Woodhead Publishing Limited (2014).
63. T. Suhara, H. Nishihara, and J. Koyama, "Electron-beam-induced refractive index change of amorphous semiconductors," *Jpn. J. Appl. Phys.* **14**(7), 1079–1080 (1975) [The authors also published their slightly expanded work with the same title in Japanese as well. See *Shinku* **19**, 20–22 (1976)].
64. H. Nishihara et al., "Direct writing of optical gratings using a scanning electron microscope," *Appl. Opt.* **17**, 2342–2345 (1978).
65. Y. Handa et al., "Scanning-electron-microscope-written gratings in chalcogenide films for optical integrated circuits," *Appl. Opt.* **18**, 248–252 (1979).
66. H. Nishihara et al., "Electron-beam directly written micro-gratings for integrated optical circuits," *Proc. SPIE* **0239**, 134–141 (1981).
67. J. Teteris and I. Kuzmina, "Amorphous chalcogenide semiconductor resists for holography and electron-beam lithography," *Proc. SPIE* **4415**, 54–59 (2001).
68. J. Teteris, "Amorphous As–S–Se semiconductor resists for holography and lithography," *J. Non-Cryst. Solids* **299–302**, 978–982 (2002).
69. M. Vlcek and H. Jain, "Nanostructuring of chalcogenide glasses using electron beam lithography," *J. Optoelectron. Adv. Mater.* **8**, 2108–2111 (2006).
70. J. R. Neilson et al., "Fabrication of nano-gratings in arsenic sulphide film," *J. Non-Cryst. Solids* **353**, 1427–1430 (2007).
71. K. Tanaka, "Electron beam induced reliefs in chalcogenide glasses," *Appl. Phys. Lett.* **70**, 261–263 (1997).
72. V. Kolbjonoks et al., "Fabrication of gratings and optical diffractive elements on chalcogenide thin films," *Proc. SPIE* **8001**, 80012P (2011).
73. V. Kolbjonoks et al., "Optical grating recording in ChG thin film by electron beam," *J. Non-Cryst. Solids* **377**, 169–171 (2013).
74. V. Bilanych et al., "Electron-beam induced surface relief shape inversion in amorphous $Ge_4As_4Se_{92}$ thin films," *Thin Solid Films* **571**, 175–179 (2014).
75. S. A. Sergeev, M. S. Iovu, and O. V. Iaseniuc, "Electron-beam recording of patterns in chalcogenide films," *Proc. SPIE* **9258**, 92580S (2015).
76. O. Shylenko et al., "Evaluation of sensitivity of $Ge_9As_9Se_{82}$ and $Ge_{16}As_{24}Se_{60}$ thin films to irradiation with electron beam," *J. Non-Cryst. Solids* **505**, 37–42 (2019).
77. A. Kumar, L. K. Malhotra, and K. L. Chopra, "Negative resist behavior of obliquely deposited Ge–Sb–Se thin films," *J. Vac. Sci. Technol. A* **5**, 354–357 (1987).
78. A. Kumar, L. K. Malhotra, and K. L. Chopra, "Photon and electron beam induced chemical solubility changes in amorphous P–Ge–Se thin films," *J. Vac. Sci. Technol. A* **6**, 2431–2433 (1988).
79. O. Shiman, V. Gerbreders, and A. Gulbis, "The interaction between electron beam and amorphous chalcogenide films," *J. Non-Cryst. Solids* **358**, 1876–1879 (2012).

80. O. Shiman et al., "The interaction between electron beam and amorphous chalcogenide films," *J. Non-Cryst. Solids* **377**, 165–168 (2013).
81. G. B. Hoffman et al., "Relief and trench formation on chalcogenide thin films using electron beams," *J. Vac. Sci. Technol. B* **26**, 2478–2483 (2008).
82. A. Yoshikawa et al., "A new inorganic electron resist of high contrast," *Appl. Phys. Lett.* **31**, 161–163 (1977).
83. K. Balasubramanyam and A. L. Ruoff, "Oblique deposition enhanced sensitivity in electron beam exposed g-Ge_xSe_{1-x} inorganic resist," *J. Vac. Sci. Technol.* **19**, 1374–1378 (1981).
84. B. Singh et al., "Sub-50-nm lithography in amorphous Se-Ge inorganic resist by electron beam exposure," *Appl. Phys. Lett.* **41**, 1002–1004 (1982).
85. K. L. Chopra et al., "Photon, electron and ion beam induced physical and optical densification in chalcogenide films," *Bull. Mater. Sci.* **6**, 1013–1018 (1984).
86. A. S. Chen et al., "Electron-beam investigation and use of Ge–Se inorganic resist," *J. Vac. Sci. Technol. B* **4**, 398–402 (1986).
87. J. Ingwersen, "Investigations on the Ag_2S/GeS_2-inorganic photoresist system for the fabrication of high resolution zone plates," in *X-Ray Microscopy III. Springer Series in Optical Sciences*, A. G. Michette, G. R. Morrison, and C. J. Buckley, Eds., Vol. 67, Springer, Berlin and Heidelberg (1992).
88. J. S. Romero, A. G. Fitzgerald, and K. Mietzsch, "Electron beam induced patterns in Ag/GeS_4," *J. Optoelectron. Adv. Mater.* **3**, 649–654 (2001)
89. J. S. Romero and A. G. Fitzgerald, "Electron-beam interactions in Cu–$GeSe_2$ amorphous thin films," *J. Appl. Phys.* **93**, 4517–4520 (2003).
90. B. Singh et al., "New inorganic electron resist system for high resolution lithography," *Appl. Phys. Lett.* **41**, 889–891 (1982).
91. G. H. Bernstein et al., "High-resolution electron beam lithography with negative organic and inorganic resists," *J. Vac. Sci. Technol. B* **6**, 2298–2302 (1988).
92. K. Mietzsch and A. G. Fitzgerald, "Electron-beam-induced patterning of thin film arsenic-based chalcogenides," *Appl. Surf. Sci.* **162–163**, 464–468 (2000).
93. G. M. Goldberg et al., "A novel high speed electron resist," in *1979 Int. Electron Devices Meeting*, pp. 62–64 (1979).
94. R. K. Debnath, A. G. Fitzgerald, and N. Nusbar, "Electron beam fabrication of masks in amorphous metal-chalcogenide bilayers," *J. Phys.: Conf. Ser.* **26**, 211–214 (2006).
95. Y.-C. Liang and K. Tada, "Silver distribution in wet-sensitized $As_{10}Ge_{22.5}Se_{67.5}$ films after electron beam exposure," *J. Appl. Phys.* **64**, 1378–1383 (1988).
96. A. G. Fitzgerald, "The origin of electron beam patterning in silver/amorphous chalcogenide bilayers," *J. Mater. Sci.* **50**, 2626–2633 (2015).
97. M. S. M. Saifullah et al., "Spin-coatable Al_2O_3 resists in electron-beam nanolithography," *Proc. SPIE* **3678**, 633–642 (1999).
98. H. Namatsu et al., "Three-dimensional siloxane resist for the formation of nanopatterns with minimum linewidth fluctuations," *J. Vac. Sci. Technol. B* **16**, 69–76 (1998).
99. K. Yamazaki et al., "Sub-10 nm electron beam lithography with sub-10 nm overlay accuracy," *Proc. SPIE* **3997**, 458–466 (2000).
100. M. S. M. Saifullah et al., "Sub-10 nm electron beam nanolithography using spin-coatable TiO_2 resists," *Nano Lett.* **3**, 1587–1591 (2003).
101. K. R. V. Subramanian et al., "Direct writing of ZrO_2 on a sub-10 nm scale using an electron beam," *Nanotechnology* **15**, 158–162 (2004).
102. M. S. M. Saifullah et al., "Spin-coatable HfO_2 resist for optical and electron beam lithographies," *J. Vac. Sci. Technol. B* **28**, 90–95 (2010).
103. M. S. M. Saifullah et al., "Effect of chelating agents on high resolution electron beam nanolithography of spin-coatable alumina gel films," *Jpn. J. Appl. Phys.* **38**, 7052–7058 (1999).
104. M. S. M. Saifullah, K. Kurihara, and C. J. Humphreys, "Comparative study of sputtered and spin-coatable aluminum oxide electron beam resists," *J. Vac. Sci. Technol. B* **18**, 2737–2744 (2000).

105. J. Fujita et al., "Nanometer-scale resolution of calixarene negative resist in electron beam lithography," *J. Vac. Sci. Technol. B* **14**, 4272–4276 (1996).
106. S.-W. Nam et al., "Contrast enhancement behavior of hydrogen silsesquioxane in a salty developer," *J. Vac. Sci. Technol. B* **27**, 2635–2639 (2009).
107. M. S. M. Saifullah et al., "Electron beam nanolithography of β-ketoester modified aluminium tri-sec-butoxide," *J. Sol-Gel Sci. Technol.* **29**, 5–10 (2004).
108. K. R. V. Subramanian, "Spin-coatable oxide resists for electron beam nanolithography," Ph.D. Thesis, University of Cambridge (2006).
109. E. Zanchetta et al., "Novel hybrid organic–inorganic spin-on resist for electron- or photon-based nanolithography with outstanding resistance to dry etching," *Adv. Mater.* **25**, 6261–6265 (2013).
110. D. Garoli et al., "Directly nanopatternable nanoporous titania: application to cell growth engineering," *Microelectron. Eng.* **155**, 102–106 (2016).
111. G. Della Giustina et al., "Electron beam lithography of hybrid sol-gel negative resist," *Microelectron. Eng.* **86**, 745–748 (2009).
112. D. Garolia and G. Della Giustina, "Directly patternable high refractive index ferroelectric sol–gel resist," *Mater. Chem. Phys.* **164**, 63–70 (2015).
113. W. J. Mitchell and E. L. Hu, "Selective area chemical vapor deposition of titanium oxide films: characterization of $Ti(OC_3H_7)_4$ as an electron beam resist," *J. Vac. Sci. Technol. B* **17**, 1622–1626 (1999).
114. W. J. Mitchell and E. L. Hu, "*In situ* electron-beam lithography on GaAs substrates using a metal alkoxide resist," *Appl. Phys. Lett.* **74**, 1916–1918 (1999).
115. W. J. Mitchell and E. L. Hu, "High-resolution in situ electron beam patterning using $Ti(OC_3H_7)_4$ as a negative-type resist," *J. Vac. Sci. Technol. B* **20**, 596–603 (2002).
116. K. Mori and S. Okamura, "Electron beam-induced structuring of composite oxides by means of dipping pyrolysis of metal naphthenate films," *Jpn. J. Appl. Phys.* **31**, L1143–L1145 (1992).
117. A. Kakimi et al., "Fabrication of ferroelectric $Bi_4Ti_3O_{12}$ thin films by dipping pyrolysis of metal naphthenates and micropatterns by an electron beam," *Jpn. J. Appl. Phys.* **33**, 5301–5304 (1994).
118. S. Okamura et al., "Micropatterning of ferroelectric $Bi_4Ti_3O_{12}$ using electron-beam-induced reaction of metal octylate films," *Jpn. J. Appl. Phys.* **35**, 6579–6583 (1996).
119. M. Alexe et al., "Patterning and switching of nanosize ferroelectric memory cells," *Appl. Phys. Lett.* **75**, 1793–1795 (1999).
120. M. Alexe et al., "100-nm lateral size ferroelectric memory cells fabricated by electron-beam direct writing," *Appl. Phys. A* **70**, 247–251 (2000).
121. S. Kiyohara et al., "Nanopatterning of diamond films with composite oxide mask of metal octylates in electron beam lithography," *J. Mater. Sci. Mater. Electron.* **15**, 99–102 (2004).
122. M. S. M. Saifullah et al., "Sub-10 nm high aspect ratio patterning of ZnO in a 500 mm main field," *J. Vac. Sci. Technol. B* **24**, 1215–1218 (2006).
123. M. S. M. Saifullah et al., "Sub-10 nm high aspect ratio patterning of ZnO by an electron beam," *Adv. Mater.* **17**, 1757–1761 (2005).
124. G. A. C. Jones, G. Xiong, and D. Anderson, "Fabrication of nanoscale ZnO field effect transistors using the functional precursor zinc neodecanoate directly as a negative electron beam lithography resist," *J. Vac. Sci. Technol. B* **27**, 3164–3168 (2009).
125. N. Tiwale et al., "Solution-processed high-performance ZnO nano-FETs fabricated with direct-write electron-beam-lithography-based top-down route," *Adv. Electron. Mater.* **7**, 2000978 (2021).
126. S. P. Patole et al., "Patterned carbon nanotube growth using an electron beam sensitive direct writable catalyst," *Nanotechnology* **20**, 315302 (2009).
127. M. Nedelcu et al., "Fabrication of sub-10 nm metallic lines of low line-width roughness by hydrogen reduction of patterned metal–organic materials," *Adv. Funct. Mater.* **20**, 2317–2323 (2010).
128. K. Bi et al., "Direct patterning of highly-conductive graphene@copper composites using copper naphthenate as a resist for graphene device applications," *Nanoscale* **9**, 16755–16763 (2017).

129. L. Berger et al., "Room temperature direct electron beam lithography in a condensed copper carboxylate," *Micromachines* **12**, 580 (2021).
130. T. Bhuvana and G. U. Kulkarni, "Highly conducting patterned Pd nanowires by direct-write electron beam lithography," *ACS Nano*, **2**, 457–462 (2008).
131. T. J. Stark et al., "Electron beam induced metalization of palladium acetate," *J. Vac. Sci. Technol. B* **9**, 3475–3478 (1991).
132. A. Chaker et al., "Nanoscale patterning of zinc oxide from zinc acetate using electron beam lithography for the preparation of hard lithographic masks," *ACS Appl. Nano Mater.* **4**, 406–413 (2021).
133. M. C. Sharps et al., "Organotin carboxylate reagents for nanopatterning: chemical transformations during direct-write electron beam processes," *Chem. Mater.* **31**, 4840–4850 (2019).
134. J. Stowers and D. A. Keszler, "High resolution, high sensitivity inorganic resists," *Microelectron. Eng.* **86**, 730–733 (2009).
135. A. Telecky et al., "Photopatternable inorganic hardmask," *J. Vac. Sci. Technol. B* **28**, C6S19–C6S22 (2010).
136. K. C. Fairley et al., "Sub-30 keV patterning of HafSOx resist: effects of voltage on resolution, contrast, and sensitivity," *J. Vac. Sci. Technol. B* **34**, 041607 (2016).
137. N. Kenane and D. A. Keszler, "High-resolution lithographic patterning with organotin films: role of CO_2 in differential dissolution rates," *ACS Appl. Mater. Interfaces* **13**, 18974–18983 (2021).
138. J. K. Stowers et al., "Directly patterned inorganic hardmask for EUV lithography," *Proc. SPIE* **7969**, 796915 (2011).
139. A. Grenville et al., "Integrated fab process for metal oxide EUV photoresist," *Proc. SPIE* **9425**, 94250S (2015).
140. Y. Zhang et al., "Dual-tone application of a tin-oxo cage photoresist under e-beam and EUV exposure," *J. Photopolym. Sci. Technol.* **31**, 249–255 (2018).
141. M. Li et al., "Novel Sn-based photoresist for high aspect ratio patterning," *Proc. SPIE* **10586**, 105860K (2018).
142. R. T. Frederick et al., "Thermal and radiation chemistry of butyltin oxo hydroxo: a model inorganic photoresist," *Microelectron. Eng.* **205**, 26–31 (2019).
143. L. Wu et al., "Hybrid EUV resists with mixed organic shells: a simple preparation method," *Eur. J. Inorg. Chem.* **2019**, 4136–4141 (2019).
144. L. Wu et al., "Mechanistic insights in Zr- and Hf-based molecular hybrid EUV photoresists," *J. Micro. Nanolithogr. MEMS MOEMS* **18**, 013504 (2019).
145. N. Thakur et al., "Stability studies on a sensitive EUV photoresist based on zinc metal oxoclusters," *J. Micro. Nanolithogr. MEMS MOEMS* **18**, 043504 (2019).
146. N. Thakur et al., "Mixed-ligand zinc-oxoclusters: efficient chemistry for high resolution nanolithography," *J. Mater. Chem. C* **8**, 14499–14506 (2020).
147. L. Wu et al., "Unravelling the effect of fluorinated ligands in hybrid EUV photoresists by x-ray spectroscopy," *J. Mater. Chem. C* **8**, 14757–14765 (2020).
148. R. Kumar et al., "Development of nickel-based negative tone metal oxide cluster resists for sub-10 nm electron beam and helium ion beam lithography," *ACS Appl. Mater. Interfaces* **12**, 19616–19624 (2020).
149. B. Radha and G. U. Kulkarni, "Patterned synthesis of Pd_4S: chemically robust electrodes and conducting etch masks," *Adv. Funct. Mater.* **20**, 879–884 (2010).
150. M. S. M. Saifullah et al., "Direct patterning of zinc sulfide on a sub-10 nanometer scale via electron beam lithography," *ACS Nano* **11**, 9920–9929 (2017).
151. J. Recatala-Gomez et al., "Thermoelectric properties of sub-stoichiometric electron beam patterned bismuth sulfide thin films," *ACS Appl. Mater. Interfaces* **12**, 33647–33655 (2020).
152. M. S. M. Saifullah et al., "Room temperature patterning of nanoscale MoS_2 under an electron beam," *ACS Appl. Mater. Interfaces* **12**, 16772–16781 (2020).
153. T. Rath et al., "Direct extreme UV-lithographic conversion of metal xanthates into nanostructured metal sulfide layers for hybrid photovoltaics," *J. Mater. Chem. A* **1**, 11135–11140 (2013).

154. W. Wang, P. Pfeiffer, and L. Schmidt-Mende, "Direct patterning of metal chalcogenide semiconductor materials," *Adv. Funct. Mater.* **30**, 2002685 (2020).
155. D. J. Webb and M. Hatzakis, "Metal methacrylates as sensitizers for poly methyl methacrylate electron resists," *J. Vac. Sci. Technol.* **16**, 2008–2013 (1979).
156. H. G. Craighead and L. M. Schiavone, "Metal deposition by electron beam exposure of an organometallic film," *Appl. Phys. Lett.* **48**, 1748–1750 (1986).
157. C. M. Chuang et al., "Nanolithography made from water-based spin-coatable LSMO resist," *Nanotechnology* **17**, 4399–4404 (2006).
158. M. C. Wu et al., "Fabrication and optical properties of periodical structures based on a water-developable and tunable $La_{0.7}Sr_{0.3}MnO_3$ resist," *J. Mater. Chem.* **18**, 780–785 (2008).
159. R. Abargues et al., "High-resolution electron-beam patternable nanocomposite containing metalnanoparticles for plasmonics," *Nanotechnology* **19**, 355308 (2008).
160. J. Marqués-Hueso et al., "Au-PVA nanocomposite negative resist for one-step three-dimensional e-beam lithography," *Langmuir* **26**, 2825–2830 (2010).
161. B-M. Lee et al., "Patterning of polymer nanocomposite resists containing metal nanoparticles by electron beam lithography," *J. Nanosci. Nanotechnol.* **11**, 7390–7393 (2011).
162. K. Bi et al., "Direct electron-beam patterning of transferrable plasmonic gold nanoparticles using a $HAuCl_4$/PVP composite resist," *Nanoscale* **11**, 1245–1252 (2019).
163. M. G. Moinuddin et al., "Functionalized Ag nanoparticles embedded in polymer resists for high-resolution lithography," *Appl. Nano Mater.* **3**, 8651–8661 (2020).
164. B-Y. Zong et al., "A general approach to semimetallic, ultra-high-resolution, electron-beam resists," *Adv. Funct. Mater.* **19**, 1437–1443 (2009).
165. C. Con, J. Zhang, and B. Cui, "Nanofabrication of high aspect ratio structures using an evaporated resist containing metal," *Nanotechnology* **25**, 175301 (2014).
166. L. F. Thompson et al., "Polymeric resists for x-ray lithography," *J. Electrochem. Soc.* **121**, 1500–1503 (1974).
167. R. D. Heidenreich and L. F. Thompson, "Electron beam generated patterns of metal-containing polymers," U.S. Patent 3,885,076 (1975).
168. M. J. MacLachlan et al., "Shaped ceramics with tunable magnetic properties from metal-containing polymers," *Science* **287**, 1460–1463 (2000).
169. S. B. Clendenning et al., "Direct writing of patterned ceramics using electron-beam lithography and metallopolymer resists," *Adv. Mater.* **16**, 215–219 (2004).
170. W. Y. Chan et al., "Highly metallized polymers: synthesis, characterization, and lithographic patterning of polyferrocenylsilanes with pendant cobalt, molybdenum, and nickel cluster substituents," *J. Am. Chem. Soc.* **127**, 1765–1772 (2005).
171. J. Zhang et al., "Metal-carbonyl organometallic polymers, PFpP, as resists for high-resolution positive and negative electron beam lithography," *Chem. Commun.* **51**, 17592–17595 (2015).
172. J. Peter et al., "Organotin in nonchemically amplified polymeric hybrid resist imparts better resolution with sensitivity for next-generation lithography," *ACS Appl. Polym. Mater.* **2**, 1790–1799 (2020).
173. A. S. Abbas et al., "Water soluble and metal-containing electron beam resist poly(sodium 4-styrenesulfonate)," *Mater. Res. Express* **1**, 045102 (2014).
174. M. T. Reetz et al., "Fabrication of metallic and bimetallic nanostructures by electron beam induced metallization of surfactant stabilized Pd and Pd/Pt clusters," *J. Am. Chem. Soc.* **119**, 4539–4540 (1997).
175. J. Lohau et al., "Electron-beam lithography with metal colloids: direct writing of metallic nanostructures," *J. Vac. Sci. Technol. B* **16**, 77–79 (1998).
176. T. R. Bedson et al., "Quantitative evaluation of electron beam writing in passivated gold nanoclusters," *Appl. Phys. Lett.* **78**, 1921–1923 (2001).
177. X. M. Lin, R. Parthasarathy, and H. M. Jaeger, "Direct patterning of self-assembled nanocrystal monolayers by electron beams," *Appl. Phys. Lett.* **78**, 1915–1917 (2001).
178. T. R. Bedson, R. E. Palmer, and J. P. Wilcoxon, "Mechanism of electron-beam writing in passivated gold nanoclusters," *Appl. Phys. Lett.* **78**, 2061–2063 (2001).
179. T. R. Bedson, R. E. Palmer, and J. P. Wilcoxon, "Electron beam lithography in passivated gold nanoclusters," *Microelectron. Eng.* **57–58**, 837–841 (2001).

180. B. F. G. Johnson et al., "Electron-beam induced formation of nanoparticle chains and wires from a ruthenium cluster polymer," *Chem. Commun.* **2000**, 1317–1318 (2000).
181. M. H. V. Werts et al., "Nanometer scale patterning of Langmuir–Blodgett films of gold nanoparticles by electron beam lithography," *Nano Lett.* **2**, 43–47 (2002).
182. C. Y. Ouyang et al., "Non-aqueous negative-tone development of inorganic metal oxide nanoparticle photoresists for next generation lithography," *Proc. SPIE* **8682**, 86820R (2013).
183. K. Kasahara et al., "Nanoparticle photoresist studies for EUV lithography," *Proc. SPIE* **10143**, 1014308 (2017).
184. V. Nandwana et al., "Direct patterning of quantum dot nanostructures via electron beam lithography," *J. Mater. Chem.* **21**, 16859–16862 (2011).
185. D. B. Dement, M. K. Quan, and V. E. Ferry, "Nanoscale patterning of colloidal nanocrystal films for nanophotonic applications using direct write electron beam lithography," *ACS Appl. Mater. Interfaces* **11**, 14970–14979 (2019).
186. Y. Wang et al., "Direct wavelength-selective optical and electron-beam lithography of functional inorganic nanomaterials," *ACS Nano* **13**, 13917–13931 (2019).
187. C. D. Dieleman et al., "Universal direct patterning of colloidal quantum dots by (extreme) ultraviolet and electron beam lithography," *Nanoscale* **12**, 11306–11316 (2020).
188. C. D. Dieleman et al., "Direct patterning of $CsPbBr_3$ nanocrystals via electron-beam lithography," *ACS Appl. Energy Mater.* **5**, 1672–1680 (2022).
189. M. Wang, W. Yueh, and K. E. Gonsalves, "New anionic photoacid generator bound polymer resists for EUV lithography," *Macromolecules* **40**, 8220–8224 (2007).
190. J. W. Thackeray et al., "Optimization of polymer-bound PAG (PBP) for 20 nm EUV lithography," *J. Photopolym. Sci. Technol.* **24**, 179–183 (2011).
191. P. G. Reddy et al., "Ferrocene bearing non-ionic poly-aryl tosylates: synthesis, characterization and electron beam lithography applications," *J. Photopolym. Sci. Technol.* **31**, 669–678 (2018).
192. V. S. V. Satyanarayana et al., "A hybrid polymeric material bearing a ferrocene-based pendant organometallic functionality: synthesis and applications in nanopatterning using EUV lithography," *RSC Adv.* **4**, 59817 (2014).
193. V. Kalyani et al., "New polyoxometalates containing hybrid polymers and their potential for nano-patterning," *Chem. Eur. J.* **21**, 2250–2258 (2015).
194. S. K. Sharma et al., "Focusing on nanoparticles-based photomultiplier in n-CARs," *Proc. SPIE* **11326**, 113261C (2020).
195. C. Dimitrakakis et al., "Top-down patterning of zeolitic imidazolate framework composite thin films by deep x-ray lithography," *Chem. Commun.* **48**, 7483–7485 (2012).
196. H. Xu et al., "Metal–organic framework-inspired metal-containing clusters for high-resolution patterning," *Chem. Mater.* **30**, 4124–4133 (2018).
197. M. Tu et al., "Direct x-ray and electron-beam lithography of halogenated zeolitic imidazolate frameworks," *Nat. Mater.* **20**, 93–99 (2021).
198. N. Tiwale et al., "Advancing next generation nanolithography with infiltration synthesis of hybrid nanocomposite resists," *J. Mater. Chem. C* **7**, 8803–8812 (2019).
199. N. Tiwale et al., "Infiltration synthesis of hybrid nanocomposite resists for advanced nanolithography," *Proc. SPIE* **11326**, 113260J (2020).
200. S. M. Hwang et al., "Photochemical study of metal infiltrated e-beam resist using vapor-phase infiltration for EUV applications," *Proc. SPIE* **11854**, 118541C (2021).
201. N. Tiwale et al., "Hybrid resist synthesis by *ex-situ* vapor-phase infiltration of metal oxides into conventional organic resists," *Proc. SPIE* **11612**, 116120A (2021).
202. M. Yasuda et al., "Computational study of pattern formation for chemically amplified resists in extreme ultraviolet lithography," *J. Photopolym. Sci. Technol.* **32**, 339 (2019).
203. M. S. M. Saifullah et al., "Approaching the resolution limit of commercial electron beam lithography – luminescent 4 nm CdS ensemble patterned using a low molecular weight resist," manuscript in preparation (2021).
204. B. Cardineau, "Chapter 11–Molecular organometallic resists for EUV (MORE)," in *Frontiers of Nanoscience*, A. Robinson and R. Lawson, Eds., Vol. 11, pp. 377–420, Elsevier, Amsterdam (2016).

205. J. Passarelli et al., "High-sensitivity molecular organometallic resist for EUV (MORE)," *Proc. SPIE* **9425**, 94250T (2015).
206. J. Passarelli et al., "Organometallic carboxylate resists for extreme ultraviolet with high sensitivity," *J. Micro. Nanolithogr. MEMS MOEMS* **14**, 043503 (2015).
207. R. Del Re et al., "Low-line edge roughness extreme ultraviolet photoresists of organotin carboxylates," *J. Micro. Nanolithogr. MEMS MOEMS* **14**, 043506 (2015).
208. M. Sortland et al., "Platinum and palladium oxalates: positive-tone extreme ultraviolet resists," *J. Micro. Nanolithogr. MEMS MOEMS* **14**, 043511 (2015).
209. J. W. Thackeray, "Materials challenges for sub-20-nm lithography," *J. Micro. Nanolithogr. MEMS MOEMS* **10**, 033009 (2011).
210. H. J. Levinson, "The potential of EUV lithography," *Proc. SPIE* **11177**, 1117702 (2019).
211. R. S. Wise, "Breaking stochastic tradeoffs with a dry deposited and dry developed EUV photoresist system," *Proc. SPIE* **11612**, 1161203 (2021).
212. J.-H. Franke et al., "Tomorrow's pitches on today's 0.33 NA scanner: pupil and imaging conditions to print P24 L/S and P28 contact holes," *Proc. SPIE* **11517**, 1151716 (2021).
213. J. G. Santaclara et al., "Today's scorecard for tomorrow's photoresist: progress and outlook towards High-NA EUV lithography," *Proc. SPIE* **11612**, 1161204 (2021).
214. V. R. Manfrinato et al., "Aberration-corrected electron beam lithography at the one nanometer length scale," *Nano Lett.* **17**, 4562–4567 (2017).

Mohammad S. M. Saifullah is a scientist at the Laboratory for Micro and Nanotechnology, Paul Scherrer Institute, Switzerland. He received his MEng degree from Department of Metallurgy, Indian Institute of Science, Bangalore, India, with a first class with distinction, in 1994. After receiving the prestigious Cambridge Nehru Scholarship, he joined the Department of Materials Science and Metallurgy, University of Cambridge, for his PhD, where he investigated metal fluorides and metal oxides for their suitability as high-resolution resists for electron and focused ion beam lithographies. After receiving his PhD in 1997, he worked at the NTT Basic Research Laboratories, Atsugi-shi (Japan), for 2 years as a researcher where he developed spin-coatable metal oxide resists capable of single digit nanoscale patterning using electron beam lithography. This was followed by demonstration of sub-10 nm direct electron beam patterning of metal sulfides at the Institute of Materials Research and Engineering (A*STAR), Singapore. He is currently developing innovative molecular resists for EUV lithography.

Nikhil Tiwale is a scientific associate in Electronic Nanomaterials Group at the Center for Functional Nanomaterials, Brookhaven National Laboratory. He received his BTech degree in metallurgical engineering and materials science, and his MTech degree in ceramics and composites at the Indian Institute of Technology Bombay in 2012. He pursued his PhD on direct-write electron beam lithography of ZnO nano-FETs and gas sensors under the supervision of Professor Sir Mark Welland at the University of Cambridge, sponsored by the Cambridge Trusts. After completing his PhD in 2017, he worked as silicon process engineer at Adaptix Ltd. He pursued postdoctoral research over 2018 to 2021 working with Dr. Chang-Yong Nam developing infiltration synthesis of hybrid EUV resists and fabrication of nanoelectronic devices.

Ramakrishnan Ganesan is an associate professor at the Department of Chemistry, Birla Institute of Technology and Science, Pilani, Hyderabad, India. He received his master's degree from Anna University, Chennai, in 2002. He received his PhD from Korea Advanced Institute of Science and Technology in 2006 under the supervision of Professor Jin-Baek Kim. During his PhD, he worked on polymeric and molecular resists for deep UV lithography and biomolecular patterning applications. He then worked at Helmholtz-Zentrum Geesthacht, Teltow, Germany, during the period of April 2008 to January 2010, where he developed polymeric materials with a special emphasis on surface functionalization toward surface endothelialization. After this, he joined as a scientist at the Institute of Materials Research and Engineering (A*STAR), Singapore. There he developed metal-containing resists for thermal and UV-mediated direct nanoimprinting of functional oxides and metals. Currently, he is actively researching in designing and developing materials for nanofabrication, photocatalysis, antimicrobial surfaces, enzymatic polymer degradation, and biosensing.